Triton Knoll Offshore Wind Farm Project

Triton Knoll Offshore Wind Farm and Export Cable Corridor Stage 3 Palaeoenvironmental Assessment

Doc No: 2505-ROH-CON-K-RA-2909497

Rev: 04

CONFIDENTIAL

For COMPANY Use Only

Review Code (Mark with X as appropriate)		**Signature of Reviewer**
Code 1 (Accepted)		
Code 2 (Accepted with Comments)		
Code 3 (Not Accepted, Do not Proceed)		
Code 4 (Rejected, Not Reviewed)		
Code 5 (Review not Required)		
Name		
Position		
Date		

For Contractor Use

04	28 August 2019	Updated following Historic England comments	Claire Mellett (Wessex Archaeology)	Dave Norcott (Wessex Archaeology)	Victoria Cooper (Royal HaskoningDHV)
03	24 May 2019	Updated following TKOWFL comments	Claire Mellett (Wessex Archaeology)	Dave Norcott (Wessex Archaeology)	Victoria Cooper (Royal HaskoningDHV)
02	05 March 2019	Updated following TKOWFL comments	Claire Mellett (Wessex Archaeology)	Dave Norcott (Wessex Archaeology)	Victoria Cooper (Royal HaskoningDHV)

01	06 Dec 2018	Issued for Review	Alex Brown and Claire Mellett (Wessex Archaeology)	Louise Tizzard (Wessex Archaeology)	Victoria Cooper (Royal HaskoningDHV)
Rev No.	**Date**	**Status/Reason for Issue**	**Author**	**Checked by**	**Approved by**

Triton Knoll Offshore Wind Farm and Export Cable Corridor

Stage 3 Palaeoenvironmental Assessment

Ref:
70076.08
August 2019

wessexarchaeology

Portway House
Old Sarum Park
Salisbury
Wiltshire
SP4 6EB

www.wessexarch.co.uk

Document Information

Document title	Triton Knoll Offshore Wind Farm and Export Cable Corridor
Document subtitle	Palaeoenvirnmental assessment
Document reference	70076.08
Client name	Royal HaskoningDHV
Address	Rightwell House, Bretton, Peterborough, Cambridgeshire, PE3 8DW
Site location	
County	
National grid reference	
Statutory designations	
Planning authority	
Planning reference	
Museum name	
Museum accession code	
WA project name	
WA project code	70076
Date of fieldwork	
Fieldwork directed by	
Project management by	Louise Tizzard
Document compiled by	Alex Brown and Claire Mellett
Contributions from	
Graphics by	

Quality Assurance

Issue and date		Status	Author	Approved by
1			ADB/CLM	DRN
2	07/11/2018	External draft	CLM	LT
3	14/02/2019	External draft	CLM	DRN
4	08/07/2019	Revised after HE comments	CLM	DRN
5	27/08/2019	Final	CLM	DRN

Contents

List of Figures

List of Tables

Summary

Wessex Archaeology (WA) was commissioned by Royal HaskoningDHV to undertake a palaeoenvironmental assessment of geotechnical samples from the Triton Knoll Offshore Wind Farm (TKOWF) and Export Cable Corridor (ECC).

The samples comprise a borehole (BH-A03a) acquired during 2015 ground investigations and located at the northwestern edge of TKOWF, and a vibrocore (VC_04) acquired during ground investigations in 2016 and located at the western end of the Export Cable Corridor.

The work comprises palaeoenvironmental assessment (pollen, foraminifera, ostracod and diatoms) and radiocarbon dating of sediment from vibrocore VC_04, with samples from borehole BH-A03a subjected to Optically Stimulated Luminescence (OSL) dating.

Pollen preservation and concentrations were excellent in all sub-samples characterised by mix broadleaved woodland dominated oak-elm-lime and hazel on the dry ground and alder-dominated fen carr woodland growing on wetter soils along the edges of channels. Saltmarsh environments are indicated nearby, consistent with the results of foraminifera and ostracod assessment that are characteristic of brackish saltmarsh and mudflats. Diatoms were poorly preserved but consistent with a marine-brackish environment.

Radiocarbon dating from VC_04 produced two inverted dates corresponding to the Allerød interstadial (14075-13771 and 13762-13484 cal. BP). The radiocarbon dates are as much as 5500–6000 years earlier than the date suggested by the pollen, which includes lime pollen unlikely to have been present in the area much before around 8000 BP.

Based on the Stage 3 assessment results presented in this report, no further Stage 4 palaeoenvironmental analysis is recommended from vibrocore VC_04 in view of the difficulty in radiocarbon dating the deposits, the lack of significant change in the pollen assemblages and the poor preservation of diatoms.

Paired quartz OSL and K-feldspar IRSL dates from a sample at 7.50 mbsf in BH-A03a returned an age between 45.7 ± 4.7 and 38.9 ± 7.6 ka which corresponds to the late-Middle to early-Upper Palaeolithic. The dates suggest deposition during the last glacial period, the Weichselian, in an ice-marginal, but terrestrial environment. The geoarchaeological potential of these deposits are therefore considered to be low and no further Stage 4 analysis is recommended.

At a depth of 26.05 mbsf in BH-A03a, paired quartz and K-feldspar IRSL dates place give an age between 152.2 ± 20.0 ka and 361.8 ± 35.6 ka, corresponding to the Saalian glacial period (MIS 10-6). The deposits are interpreted to have been deposited in an emergent southern North Sea and are therefore of archaeological interest. However, the coarse-grained nature of deposits means the potential for preservation of palaeoenvironmental material is low and no further Stage 4 analysis is recommended.

Acknowledgements

This work was commissioned by Royal HaskoningDHV, on behalf of Triton Knoll Offshore Wind Farm Ltd. The assistance of Victoria Cooper of Royal HaskoningDHV and Dr Leo James of Triton Knoll Offshore Wind Farm Ltd. during the production of this report is acknowledged.

The report was compiled by Dr Alex Brown and Dr Claire Mellett. Illustrations were prepared by Ken Lymer. Quality control was provided by Dr Louise Tizzard who managed the project for Wessex Archaeology.

Triton Knoll Offshore Wind Farm and Export Cable Corridor

Palaeoenvironmental assessment

1 INTRODUCTION

1.1 Project background

1.1.1 Wessex Archaeology (WA) was commissioned by Royal HaskoningDHV to undertake a palaeoenvironmental assessment of geotechnical samples from the Triton Knoll Offshore Wind Farm (TKOWF) and Export Cable Corridor (ECC).

1.1.2 The samples comprise a borehole (**BH-A03a**) acquired during 2015 ground investigations and located at the northwester edge of TKOWF, and a vibrocore (**VC_04**) acquired during ground investigations in 2016 and located at the western end of the Export Cable Corridor (**Figure 1** in **Appendix 1**).

1.1.3 The work comprises palaeoenvironmental assessment (pollen, foraminifera, ostracod and diatoms) and radiocarbon dating of sediment from vibrocore **VC_04**, with samples from borehole **BHA-03a** subjected to optically stimulated luminescence dating.

1.1.4 The TKOWF site is located within the southern North Sea basin, approximately 33 km off the Lincolnshire coast and 48 km off the north Norfolk coast. The associated ECC extends from the southwest of TKOWF and covers approximately 47km to the landfall site north of Anderby Creek, Lincolnshire (**Figure 1** in **Appendix 1**).

1.2 Scope of work

1.2.1 To help frame geoarchaeological investigations of this nature, WA has developed a five-stage approach, encompassing different levels of investigation appropriate to the results obtained, accompanied by formal reporting of the results at the level achieved. The stages are summarised below (**Table 1**).

1.2.2 This palaeoenvironmental assessment represents Stage 3 of this process and details the results of work recommended in the Stage 2 report (WA 2017), with recommendations for further palaeoenvironmental analysis and reporting at Stage 4 and 5.

Table 1 Stages of geoarchaeological assessment and recording

Stage	Method	Description
1	Review	A desk-based archaeological review of the borehole, vibrocore and CPT logs generated by geotechnical contractors. Aims to establish the likely presence of horizons of archaeological interest and broadly characterise them, as a basis for deciding whether and what Stage 2 archaeological recording is required. The Stage 1 report will state the scale of Stage 2 work proposed**.**

Stage	Method	Description
2	Geoarchaeological Recording	Archaeological recording of selected retained or new core samples will be undertaken. This will entail the splitting of the cores, with each core being cleaned and recorded. The Stage 2 report will state the results of the archaeological recording and will indicate whether any Stage 3 work is warranted.
3	Sampling and Assessment	Dependent upon the results of Stage 2, sub-sampling and palaeoenvironmental assessment (pollen, diatoms and foraminifera) may be required. Subsamples will be taken if required. Assessment will comprise laboratory analysis of the samples to a level sufficient to enable the value of the palaeoenvironmental material surviving within the cores to be identified. Subsamples will also be taken and/or retained at this stage in case scientific dating is required during Stage 4. Some scientific dating (e.g. radiocarbon or Optically Stimulated Luminescence (OSL)) may be undertaken at this stage to provide chronological context. The Stage 3 report will set out the results of each laboratory assessment together with an outline of the archaeological implications of the combined results, and will indicate whether any Stage 4 work is warranted.
4	Analysis and Dating	Full analysis of pollen, diatoms and/or foraminifera assessed during Stage 3 will be undertaken. Typically, Stage 4 will be supported by scientific dating (e.g. radiocarbon or OSL) of suitable subsamples. Stage 4 will result in an account of the successive environments within the coring area, a model of environmental change over time, and an outline of the archaeological implications of the analysis.
5	Final Report	If required Stage 5 will comprise the production of a final report of the results of the previous phases of work for publication in an appropriate journal. This report will be compiled after the final phase of archaeological work, whichever phase that is.

1.3 Previous geoarchaeological work

1.3.1 Geoarchaeological works in in support of the TKOWF and Export Cable Corridor have been ongoing since 2009 (**Table 2**). Works have included desk based assessments and reviews of published literature and legacy geotechnical and geophysical data. Targeted geotechnical and geophysical surveys have been undertaken at various stages of the development and, where appropriate, WA have liaised closely with the developer throughout to maximise the outputs from these surveys.

1.3.2 In terms of geoarchaeological assessment, Stage 1 borehole reviews have been undertaken on boreholes and vibrocores recovered during three separate geotechnical surveys (WA 2009; 2016a; 2016b).

1.3.3 In 2009, 11 boreholes logs were reviewed by WA (WA 2009) and seventeen core liners from two boreholes (**BH-E** and **BH-G**) were recommended for Stage 2 geoarchaeological recording (WA 2010). Stage 2 works identified deposits associated with Sand Hole Formation (Holsteinian), Egmond Ground Formation (Late Holsteinian to Early Saalian) and Botney Cut (early Holocene) which were considered to be of archaeological interest. However, the sample depths of interest were not fully recorded, and it was recommended

that additional boreholes were obtained to provide suitable material for Stage 3 paleoenvironmental assessment.

1.3.4 In October 2015, a further seven boreholes were acquired from the TKOWF. After the 2009 Stage 1 review, WA recommended one borehole was drilled in close proximity to **BH-E** and **BH-G** to recover samples for archaeological purposes. This was outlined in the Written Scheme of Investigation (WSI) (WA 2015) and **BH-A03a** was the resulting borehole. A Stage 1 review of all 2015 boreholes was undertaken (WA 2016a) which identified thick sequences of Sand Hole Formation (Holstenian) and Egmond Ground Formation (Late Holsteinian to Early Saalian). Recommendations were made to retain core samples from these units of archaeological interest for Optical Stimulated Luminescence dating (**BH-A03a** and **BH-A09**).

1.3.5 In July 2016, a geotechnical survey comprising 10 boreholes and 44 vibrocores was undertaken and WA carried out Stage 1 geotechnical data review (WA 2016b). Again, thick sequences of Sand Hole Formation (Holstenian) and Egmond Ground Formation (Late Holsteinian to Early Saalian) were recovered. In addition, deposits of possible early Holocene age from palaeochannel features identified on geophysical data were identified in **BH_079**, **VC_04**, **VC_06**, **VC_16**, **VC_17** and **VC_46** and recommendations for Stage 2 geoarchaeological recording and deposit modelling were made. Vibrocore **VC_09** was also recommended for Stage 2 recording as organic staining was indicated on the geotechnical log.

1.3.6 In September and October 2017, a Stage 2 geoarchaeological recording of geotechnical samples was undertaken, comprising 26 samples from two boreholes (**BHA-03a** and **BHA-09**) acquired in 2015 and five vibrocores (**VC_04, VC_06, VC_09, VC_17** and **VC_46**) acquired in 2016. Recommendations for Stage 3 palaeoenvironmental assessment were made, focusing on OSL dating of Sand Holocene Formation deposits of Holsteinian date in borehole **BHA-03a** and palaeoenvironmental assessment and radiocarbon dating of possible early Holocene deposits from vibrocore **VC_04**.

1.3.7 The Stage 3 work presented here forms part of ongoing investigations in advance of the construction of the wind farm, and is based directly on recommendations made during the previous Stage 1 geoarchaeological reviews of the 2015 and 2016 geotechnical logs (WA 2016a, WA 2016b) and Stage 2 geoarchaeological recording of boreholes and vibrocores (WA 2018), as summarised above. Geoarchaeological works have been undertaken in accordance with the previously produced WSI for offshore archaeology (Royal HaskoningDHV 2016a) and with the archaeological method statement for offshore geotechnical site investigations (Royal HaskoningDHV 2016b).

Table 2 Previous geoarchaeological works in support of TKOWF and Export Cable Corridor

Report type	Title	Report no.	Geotechnical survey campaign and data assessed	Reference
Stage 1	Triton Knoll Geoarchaeology: note on cores	70070	2009 (11 boreholes)	WA 2009
Stage 2	Triton Knoll Offshore Wind Farm, Stage 2 Geoarchaeological Recording of Borehole Samples	70070.01	2009 (2 boreholes)	WA 2010

Report type	Title	Report no.	Geotechnical survey campaign and data assessed	Reference
Stage 1	Triton Knoll Offshore Wind Farm, Stage 1 Geoarchaeological Assessment of Geotechnical Logs	70076.04	2015 (7 boreholes)	WA 2016a
Stage 1	Triton Knoll Offshore Wind Farm and Export Cable Corridor, Stage 1 Archaeological Assessment of 2016 Geotechnical Logs	70076.05	2016 (10 boreholes 44 vibrocores)	WA 2016b
Stage 2	Triton Knoll Offshore Wind Farm and Export Cable Corridor, Stage 2 Geoarchaeological Recording of Geotechnical Samples	70076.06	2015 and 2016 (2 boreholes 5 vibrocores)	WA 2018
Stage 1/2	Stage 1 Review and Stage 2 Geoarchaeological Recoding of 2017-2018 Geotechnical Samples	70076.07	2017-2018 survey (20 vibrocores)	WA 2018

2 AIMS AND OBJECTIVES

2.1.1 The aim of this work is to undertake palaeoenvironmental assessment and scientific dating of deposits identified at Stage 2 to possess the most geoarchaeological potential, informing further Stage 4 analysis and Stage 5 final reporting. Stage 3 work is undertaken in accordance with the WSI (Royal HaskoningDHV, 2016a) and method statement (Royal HaskoningDHV, 2016b) building upon previous Stage 1 and 2 reports (WA 2016a, 2016b, 2018).

2.1.2 The aims of the palaeoenvironmental assessment are as follows:

- Determine the potential of palaeoenvironmental remains preserved in vibrocore **VC_04**;
- Determine the age of accumulated deposits in vibrocore **VC_04** and borehole **BHA-03a**, and;
- Report on results, making suitable recommendations for further Stage 4 analysis and Stage 5 final reporting.

2.1.3 These aims will be addressed by achieving through the following objectives:

- Undertake an assessment of palaeoenvironmental remains (pollen, foraminifera, ostracod and diatoms) from vibrocore **VC_04**, focusing on preservation and concentration, and providing preliminary data on environment, vegetation change and evidence for anthropogenic impact, and;
- Submit samples for radiocarbon dating from vibrocore **VC_04**, and for optically stimulated luminescence dating (OSL) from borehole **BHA-03**.

2.1.4 Specific research questions include:

- Are quartz OSL and K-feldspar Infrared Stimulated Luminescence (IRSL) viable techniques for dating deposits of Holsteinian age, and;

- Do organo-mineral deposits preserved within Holocene palaeochannels (as represented in vibrocore **VC_04**) produce viable chronologies and palaeoenvironmental data.

3 GEOARCHAEOLOGICAL BACKGROUND

3.1.1 A full geological baseline of TKOWF is provided in the desk-based assessment (DBA) (WA 2011) and will not be repeated in detail here. However, a summary baseline of previous work associated with TKOWF is provided below.

3.1.2 The dominant solid geology of the region is the Chalk Group, an extensive deposit of chalk present throughout much of the North Sea and southern England, which was laid down in shallow marine conditions during the Upper Cretaceous period. The upper surface of the Chalk Group is erosional, and the unit is unconformably overlain by Pleistocene and, in some places, Early Holocene sediments (Cameron *et al*. 1992). These Pleistocene and Early Holocene sediments have the most relevance to geoarchaeology in the area.

3.1.3 Previous geoarchaeological assessments of boreholes from within TKOWF were undertaken by WA in 2010 and 2016 (WA 2010, 2016a, 2016b). These assessments, alongside interpretations of shallow seismic data and background information from the area, identified a shallow geological sequence comprising eight individual geological units (WA 2016a, WA 2016b).

3.1.4 A full site wide stratigraphy and deposit model for the site has since created by Fugro (Fugro 2016d, 2016e, 2016f). In order to maintain consistency with other parts of the wider project, the archaeological work has been compared and revised to correlate to this site wide stratigraphy and deposit model although, from an archaeological perspective, a number of the interpreted sub-units can be merged (**Table 3**).

3.1.5 The WA stratigraphic unit numbers presented in **Table 3** have been updated and refined and differ slightly from those used in previous reports (WA 2016a, 2016b). In addition, previous WA reports have used UK nomenclature for the description of glacial and interglacial periods. From this report, onwards, Continental European nomenclature will be used for easier correlation with the wider project (e.g. geotechnical); the corresponding British terminology is provided in **Table 3**.

3.1.6 **Unit 1** represents the Cretaceous bedrock and, as such, is too old to be of archaeological potential. **Unit 2** represents the first evidence of glaciation within the North Sea, and is characterised by a number of large, sub-glacial valleys filled with sediments of glacial origin. Due to the glacial nature of these sediments, **Unit 2** is also not considered to be of archaeological potential.

3.1.7 **Unit 3** and **Unit 4** represent a transition from fully terrestrial conditions in the area through lagoon sediments (**Unit 3**) to shallow marine (**Unit 4**) during the Holsteinian interglacial, a period within which the southern North Sea will have been suitable for hominin occupation. **Unit 3** has previously been shown to contain preserved organic material of potential palaeoenvironmental importance (Fugro 2009, WA 2010), and both **Unit 3** and **Unit 4** have the potential to contain derived archaeological artefacts or preserved *in situ* archaeological material where they cover previous land surfaces.

3.1.8 **Unit 5** is a unit of glacial till, and has been sub-divided into four sub-units by Fugro (2016d); a lower set of channels and sandy channel fill created by pro-glacial fluvial features during ice sheet advance (e), an initial subglacial till deposited after the advance (f), a second set of sandy channel fills created due to a brief period of ice sheet retreat during the Weichselian Hiatus (g), and an upper subglacial till deposited during the final Withernsea Advance (h). However, all of these sub-units were deposited either directly beneath or in close proximity to an ice sheet, during which time the study area will have been uninhabitable by human communities. As such, from an archaeological perspective, these sub-units have been grouped together as **Unit 5**, which is not considered to be of geoarchaeological potential. A series of figures illustrating this sequence has been produced by Fugro as part of the deposit model of the area (Fugro 2016d).

3.1.9 **Unit 6** has been identified as shallow channel features within previous geophysical assessments (WA 2011, 2017), and is interpreted as representing the remnants of a terrestrial landscape present in the area between the Late Glacial Maximum (LGM) and the final Holocene marine transgression. As such, these channel features and their associated deposits are considered to be of geoarchaeological potential. **Unit 6** now also contains features previously ascribed by WA to the Botney Cut Formation (**formerly Units 6 and 7a**).

3.1.10 **Unit 7** represents the modern seabed sediment deposited since the Holocene marine transgression. While it has the potential to cover archaeological sites such as shipwrecks, **Unit 7** is not considered of geoarchaeological potential.

Table 3 Interpreted stratigraphy of TKOWF. Continental European nomenclature is used in this report, but the accompanying British terminology is also provided.

WA Unit	TKOWF Stage	Period (Continental/British)		Description	Previous WA Unit
7	j	Late Holocene		Undifferentiated Holocene marine gravelly sands/sandy gravels	7b
6	i	Early Holocene		Terrestrial marshland/fluvial channels and related deposits (Elbow Formation), and Early Holocene Channels (Botney Cut Formation)	6 & 7a
5	h	Late Weichselian	Late Devensian	Sandy gravelly till (Upper Bolders Bank Formation)	5
	g			Sandy, redeposited, pro-glacial channel fill (Bolders Bank Formation Sand)	
	f			Sandy gravelly till (Lower Bolders Bank Formation)	
	e	Middle to Late Weichselian	Middle to late Devensian	Sandy, redeposited, pro-glacial channel fill (Bolders Bank Formation Channels)	
4	d	Late Holsteinian to Early Saalian	Hoxnian	Cold, deeper marine sand with layers of laminated clay (Egmond Ground Formation)	4
3	c	Early to Late Holsteinian	Hoxnian	Shallow, temperate marine/lagoon sandy laminated clays and silts with organic material (Upper Sand Hole Formation)	3

WA Unit	TKOWF Stage	Period (Continental/British)		Description	Previous WA Unit
	b	Early Holsteinian	Hoxnian	Shallow, temperate marine/lagoon laminated clays and silts with frequent organic material (Lower Sand Hole Formation)	
2	a	Middle to End Elsterian	Anglian	Redeposited glacial till overlain by pebbly glaciolacustrine / glaciomarine muds (Swarte Bank Formation)	2
1	-	Upper Cretaceous		Chalk Group (bedrock)	1

4 METHODS

4.1 Stage 3 assessment

4.1.1 Two sequences were selected for Stage 3 assessment, comprising vibrocore **VC_04** and Borehole **BHA-03a** (**Figure 1** in **Appendix 1**). The Holocene sediments in vibrocore **VC_04** showed the most potential for palaeoenvironmental assessment and radiocarbon dating, with the Pleistocene deposits in borehole **BHA-03a** selected for paired quartz OSL and K-feldspar IRSL dating. Processing methods are outlined below; all sub-sample depths are quoted as metres below sea bed (mbsb).

4.2 Radiocarbon dating

4.2.1 Two sub-samples were taken for radiocarbon dating (**Table 4**). Suitable material was identified under microscope, stored in glass tubes, with samples sent for dating to the 14CHRONO Centre at Queens University Belfast. Calibrated age ranges were calculated with OxCal 4.1 (Bronk-Ramsey and Lee 2013) using the IntCal13 curve (Reimer et al. 2013). All radiocarbon dates are quoted as uncalibrated years before present (BP), followed by the lab code and the calibrated date-range (cal. BC) at the 2σ (95.4%) confidence.

4.3 OSL

Core handling, storage and sample selection

4.3.1 Borehole samples were collected in opaque metal liners of 1.0 m length and 0.07 m diameter (shelby tubes) which were sealed offshore and transported to Wessex Archaeology. A total of five shelby tubes from **BH-A03a** were available for OSL dating.

4.3.2 As cores were not opened or described, the selection of samples for OSL dating relied on the geotechnical log constructed from intermittent borehole sampling and Cone Penetration Test (CPT) results.

4.3.3 Shelby tubes from 7.50-8.15 mbsf and 26.05-26.90 mbsf were selected for OSL dating. These samples represent the shallowest and deepest parts of the sequence and therefore have the potential to capture the greatest age range.

4.3.4 Shelby tubes selected for dating were delivered to the OSL laboratory at the University of Gloucester.

Sample preparation and analysis

4.3.5 Given the age of deposits of archaeological interest are expected to be at the maximum age limit of the quartz OSL dating technique, a paired quartz OSL and K-feldspar IRSL approach was adopted as feldspar has greater potential to accumulate signals over longer

periods of time, possibly extending the dating range beyond the Late Pleistocene. Furthermore, paired quartz OSL and K-feldspar IRSL dates provide an independent chronological control to test the accuracy of the ages produced.

4.3.1 Samples were extruded under controlled laboratory illumination provided by Encapsulite RB-10 (red) filters. Sediment located within 10 mm of each core face was carefully removed to target the centre of the core that had not been disturbed during the drilling process.

4.3.2 The remaining sample was dried and then sieved. The fine sand fraction was segregated and subjected to acid and alkaline digestion (10% HCl, 15% H_2O_2) to attain removal of carbonate and organic components respectively.

4.3.3 The sample was then divided in two. For one half, a further acid digestion in HF (40%, 60 mins) was used to etch the outer 10-15 µm layer affected by α radiation and degrade each samples' feldspar content. During HF treatment, continuous magnetic stirring was used to effect isotropic etching of grains. 10% HCl was then added to remove acid soluble fluorides. Each sample was dried, resieved and quartz isolated from the remaining heavy mineral fraction using a sodium polytungstate density separation at 2.68g.cm^{-3}. For the second half, density separations at 2.53 and 2.58 g cm^{-3} were undertaken to isolate the K-feldspar fraction.

4.3.4 Twelve 8 mm multi-grain aliquots (c. 3-6 mg) of quartz and K-feldspar were then mounted on aluminium discs for determination of D_e values.

4.3.5 All drying was conducted at 40°C to prevent thermal erosion of the signal. All acids and alkalis were Analar grade. All dilutions (removing toxic-corrosive and non-minerogenic luminescence-bearing substances) were conducted with distilled water to prevent signal contamination by extraneous particles.

4.3.6 Equivalent dose (D_e) was determined using the single-aliquot regenerative-dose (SAR) protocol (Murray and Wintle 2000, 2003 for quartz; Li et al., 2014 for K-feldspar). Lithogenic Dose Rate (D_r) values were defined through measurement of U, Th and K radionuclide concentration and conversion of these quantities into β and γ Dr values (Adamiec and Aitken, 1998), accounting for D_r modulation forced by grain size (Mejdahl, 1979) and present moisture content (Zimmerman, 1971) (**Table 5**). Cosmogenic D_r values were calculated on the basis of sample depth, geographical position and matrix density (Prescott and Hutton, 1994). Note, no *in situ* γ spectrometry was undertaken due to these samples being collected offshore, therefore the level of U disequilibrium was estimated by laboratory-based Ge γ spectrometry.

4.3.7 Ages reported in **Table 5** provide an estimate of sediment burial period based on mean D_e and D_r values and their associated analytical uncertainties. Full OSL results are presented in **Appendix 2**.

4.4 Pollen and spores

4.4.1 Eight sub-samples of 1ml volume were processed from vibrocore **VC_04** using standard pollen extraction methods (Moore et al 1991). Pollen was identified and counted using a Nikon eclipse E400 biological research microscope. A total of 150 pollen grains was counted for each sub-sample in addition to aquatics and fern spores, and where 150 counts were not possible, all pollen and spores were counted from four transects. One *Lycopodium* tablet was added to enable calculation of pollen concentrations. Pollen and spores were identified to the lowest possible taxonomic level. Plant nomenclature followed Stace (1997) and Bennett et al (1994). Pollen sums are based on total land pollen (TLP) excluding

aquatics and fern spores which are calculated as a percentage of TLP plus the sum of the component taxa within the respective category. Identification of indeterminable grains was according to Cushing (1967). At assessment stage the results are not presented as pollen diagrams but are presented in tabular form as raw data (**Table 6**).

4.5 Diatoms

4.5.1 Eight sub-samples were prepared from vibrocore **VC_04** (**Table 7**) following standard techniques (Battarbee et al 2001). Two coverslips were made from each sample and fixed in Naphrax for diatom microscopy. A large area of the coverslips on each slide was scanned for diatoms at magnifications of x400 and x1000 under phase contrast illumination.

4.5.2 Diatom floras and taxonomic publications were consulted to assist with diatom identification; these include Hendey (1964), Werff & Huls (1957-1974), Hartley *et al.* (1996), Krammer & Lange-Bertalot (1986-1991) and Witkowski *et al.* (2000). Diatom species' salinity preferences are indicated using the halobian groups of Hustedt (1953, 1957: 199), these salinity groups are summarised as follows:

1. Polyhalobian: >30g l-1

2. Mesohalobian: 0.2-30g l-1

3. Oligohalobian - Halophilous: optimum in slightly brackish water

4. Oligohalobian - Indifferent: optimum in freshwater but tolerant of slightly brackish water

5. Halophobous: exclusively freshwater

6. Unknown: taxa of unknown salinity preference.

4.6 Foraminifera and ostracod

4.6.1 Eight sub-samples were processed for foraminifera and ostracod analysis from vibrocore **VC_04** (**Table 8**).

4.6.2 The sub-samples were weighed, then broken into small pieces by hand, placed into ceramic bowls, and dried in an oven. Boiling-hot water was then poured over them with a little sodium carbonate added to help disaggregate the clay fraction. Each was left to soak overnight. It was found that breakdown was aided, especially with the organic-rich samples, by re-heating the still soaking samples in the oven for several hours before attempting to wash them. The peats, however, needed processing twice and even then, breakdown was not entirely satisfactory.

4.6.3 Sub-samples were then washed through a 75µm sieve with the remaining residue returned to the ceramic bowl for final drying in the oven. The residues were then stored in labelled plastic bags. For examination, each sample was placed in a nest of sieves (>50, >150, >250µm, and base pan) and thoroughly shaken. Each grade was then sprinkled onto a picking tray, a little at a time, and viewed under a binocular microscope. “Contained material” were logged on a presence(x)/absence basis and is shown in the accompanying **Table 8**.

4.6.4 The abundance of each foraminiferal and ostracod species was estimated semi-quantitatively (one specimen, several specimens, common and abundant/superabundant) by experience and by eye), and colour-coded to provide further ready environmental

information. Species identification comes from Murray (2006) for the foraminifera, Athersuch et al. (1989) for the brackish and marine ostracods, and Meisch (2000) for the freshwater ostracods, in addition to expert judgement.

5 RESULTS

5.1 Radiocarbon dating

5.1.1 Two sub-samples were sent for radiocarbon dating from vibrocore **VC_04** (**Table 4**). Not only are the dates inverted, but the late-glacial ages are inconsistent with the pollen that includes a range of thermophilous taxa unequivocally characteristic of the Holocene. Taxa such as *Tilia* (lime) are unlikely to have been present in this area much before approximately 8000 BP (Brewer et al 2017). The dates are therefore considered too old and unreliable as an indicator of the age of the sediment, perhaps derived on material of late glacial date eroded and reincorporated into a Holocene palaeochannel.

Table 4 AMS radiocarbon dating results, vibrocore **VC_04**

Laboratory No	Material dated	Depth (mbgs)	Age B.P	Age range cal. BC (95.4%)	Age range cal. BP (95.4%)
UB-36740	Bulk sediment	2.52-2.54	12073±48	12125-11821	14075-13771
UB-36741	Bulk sediment	3.56-3.58	11816±63	11812-11534	13762-13484

5.2 OSL dating

5.2.1 Two sub-samples from **BH-A03a** were submitted for quartz OSL and K-feldspar IRSL dating, providing two dates from a depth of 7.50 mbsf and two from 26.05 mbsf. Age data are presented in **Table 5** and full results are given in **Appendix 2**.

Table 5 Dose Rate (D_r), Equivalent Dose (D_e) and resulting OSL age estimates. Age estimates expressed in ka relative to year of sampling. Uncertainties in age are quoted at 1σ confidence and include combined systematic and experimental variability.

Laboratory id	Core	Depth mbsf	Total D_r (Gy.ka-1)	D_e (Gy)	Age (ka)	Considerations and analytical validity
GL17150 Quartz	BH-A03a	7.50	1.50 ± 0.15	58.3 ± 9.6	38.9 ± 7.6	Significant feldspar contamination. Accept as minimum age.
GL17150 K-Feldspar	BH-A03a	7.50	2.07 ± 0.18	94.3 ± 4.9	45.7 ± 4.7	Failed dose recovery test. Accept as maximum age.
GL18025 Quartz	BH-A03a	26.05	1.82 ± 0.16	276.9 ± 26.9	152.2 ± 20.0	Significant feldspar contamination. Accept as minimum age.
GL18025 K-Feldspar	BH-A03a	26.05	2.38 ± 0.19	862.5 ± 47.8	361.8 ± 35.6	Failed dose recovery test. Accept as maximum age.

5.2.2 Diagnostics were used to estimate the influence of laboratory and environmental factors on the results as a means of testing the analytical validity of the OSL age.

5.2.3 Both quartz dates showed evidence of significant feldspar contamination which is rarely a function of sample preparation as it predominantly results from the occurrence of feldspar as inclusions within the quartz. Where there is evidence of feldspar contamination, dates

are accepted as a minimum age estimate i.e. the burial age may be older but it is unlikely to be younger.

5.2.4 Both K-feldspar dates failed the dose recovery test which is used to assess the optimal preheat temperature for accurate correction and calibration of the time-dependent signal. The OSL signal may therefore have been influenced by the laboratory protocol and the age is considered a maximum estimate i.e. the burial age may be younger but is unlikely to be older.

5.2.5 The age of the deposits at 7.50 mbsf in **BH-A03a** is between 45.7 ± 4.7 and 38.9 ± 7.6 ka (**Table 5**) which corresponds to Marine Isotope Stage (MIS) 3 during the late-Middle to early-Upper Palaeolithic. Despite analytical considerations, the quartz and K-feldspar ages overlap within error margins increasing confidence in the age estimates.

5.2.6 At a depth of 26.05 mbsf, the quartz date gives a minimum age of 152.2 ± 20.0 ka while the K-feldspar date provides a maximum age of 361.8 ± 35.6 ka. This suggests the deposits at this depth were laid down at some time between MIS 6 and MIS 10 during the Saalian

5.3 Pollen and spores

5.3.1 The results of pollen assessment of vibrocore **VC_04** are presented here (**Table 6**), detailing preservation and concentration of pollen grains (palynomorphs) accompanied by an outline of the range of taxa recorded.

5.3.2 Pollen preservation and concentrations were excellent in all sub-samples (**Table 6**). The samples are dominated by arboreal pollen (ranging between 72.8–93.5%), largely variable quantities of *Quercus* (oak), *Corylus avellana* type (hazel) and *Alnus glutinosa* (alder), with smaller quantities of *Pinus sylvestris* (pine), *Betula* (birch), *Ulmus* (elm), *Tilia* (lime), *Fraxinus* (ash) and *Salix* (Willow). Non-arboreal pollen ranges between a minimum of 6.5% (2.97mbsb) and a maximum of 25.8% (3.32mbsb), but in most samples, ranges between 10.7–18.7%). Non-arboreal pollen is represented largely by Chenopodiaceae (goosefoot family), with smaller quantities of Poaceae (grass family), Cyperaceae (sedge family) and several other herbs (e.g. *Filipendula* – meadowsweet; *Aster* type – daisies).

5.3.3 Fern spores occur in small quantities, comprising a mix of Pteropsida (undifferentiated fern spores) and *Pteridium aquilinum* (bracken). Aquatic pollen taxa are largely absent apart from a single grain of *Sparganium emersum* type (unbranched bur-reed) at 2.87mbsb.

Table 6 Results of pollen assessment (%), vibrocore **VC_04**.

Taxon / **Depth (mbsb)**	**2.52**	**2.64**	**2.75**	**2.87**	**2.97**	**3.32**	**3.44**	**3.56**
Betula (birch)	7	6	6	9	5	6	3	2
Pinus sylvestris (pine)	5	5	9	5	1	6	7	3
Corylus avellana type (hazel)	48	26	36	39	24	36	51	46
Ulmus (elm)	4	2	6	2	2	3	2	-
Quercus (oak)	31	69	25	44	97	32	41	15
Tilia (lime)	5	5	3	3	-	2	2	1
Alnus glutinosa (alder)	21	11	40	32	11	23	22	67
Fraxinus excelsior (ash)	-	3	2	-	2	2	1	1
Salix (willow)	-	1	-	-	3	-	1	-
Hedera helix (ivy)	-	-	1	-	-	-	-	-

Taxon / Depth (mbsb)	2.52	2.64	2.75	2.87	2.97	3.32	3.44	3.56
Ericaceae (heather family)	1	-	-	-	-	2	-	1
Poaceae (grass family)	5	2	3	2	1	12	7	3
Cyperaceae (sedge family)	3	1	-	1	-	1	1	-
Chenopodiaceae (goosefoot family)	15	15	18	12	9	22	10	15
Artemisia type (mugworts)	-	1	-	-	-	1	-	-
Brassicaceae (cabbage family)	-	-	-	-	-	-	-	1
Rosaceae (rose family)	-	-	1	-	-	-	1	-
Filipendula (meadowsweet)	1	2	-	-	-	-	-	-
Plantago lanceolata (ribwort plantain)	-	-	-	-	-	1	-	-
Plantago media-major (hoary-greater plantain)	1	-	-	-	-	-	-	-
Rubiaceae (bedstraw family)	-	-	-	-	-	1	-	-
Lactuceae (lettuce family)	-	-	-	1	-	-	1	-
Armeria maritima (sea thrift)	1	-	-	-	-	-	-	-
Aster type (daisies)	2	1	-	-	-	1	-	-
Pteropsida undiff. (undifferentiated fern spores)	4	2	3	5	1	3	4	2
Pteridium aquilinum (bracken)	3	1	-	-	-	3	4	2
Polypodium vulgare (polypody)	-	-	1	1	-	-	-	-
Sparganium emersum type (unbranched bur-reed)	-	-	-	1	-	-	-	-
Sphagnum (bog moss)	-	-	-	-	1	2	1	-
Indeterminables	33	9	24	0	0	24	36	18
Total Land Pollen (TLP)	**150**	**150**	**150**	**150**	**155**	**151**	**150**	**155**
Arboreal pollen (%)	**80.7**	**85.3**	**84.7**	**89.3**	**93.5**	**72.8**	**86.7**	**87.1**
Non-arboreal pollen (%)	**19.3**	**14.7**	**14.7**	**10.7**	**6.5**	**27.2**	**13.3**	**12.9**
Preservation	**2**	**2**	**2**	**2**	**2**	**2**	**2**	**2**
Concentration	**1**	**1**	**1**	**1**	**1**	**1**	**1**	**1**

Preservation and Concentration: 1 = Excellent, 2 = Good, 3 = Moderate, 4 = Poor, 5 = Very poor/absent

5.4 Diatoms

5.4.1 Eight sub-samples from **VC_04** were assessed for diatoms. Diatoms are present in all eight sub-samples from the sequence. The concentrations of diatom valves are low, and in two samples (2.87 and 2.97 mbsb) the numbers of diatoms are very low. The quality of diatom preservation varies from poor to moderate in five sub-samples, and very poor in three sub-samples (2.87, 2.97 and 3.44 mbsb). The diversity of the diatom assemblages is moderately high or moderate to low in sub-samples from 2.52 to 2.75, 3.32 and 3.56 mbsb. Diatom diversity is relatively low in sub-samples from 2.87, 2.97 and 3.44 mbsb.

5.4.2 The relatively poor preservation of diatoms in several of the sub-samples from the TKOWF can be attributed to taphonomic processes (Flower 1993, Ryves *et al.* 2001). This may be the result of diatom silica dissolution and breakage caused by factors such as extremes of sediment salinity, alkalinity or acidity, the under-saturation of sediment pore water with dissolved silica, cycles of prolonged drying and rehydration, movement of water, or physical damage to diatom valves from abrasion or wave action.

Table 7 Results of diatom assessment, vibrocore **VC_04**.

Taxon	Depth (mbsb)	2.52	2.64	2.75	2.87	2.97	3.32	3.44	3.56
Polyhalobous									
Biddulphia aurita		-	-	-	1	-	-	-	-
Grammatophora sp.		-	-	1	-	-	-	1	-
Plagiogramma staurophorum		1	-	-	-	-	-	-	-
Paralia sulcata		3	3	3	3	3	3	3	3
Podosira stelligera		-	-	-	-	-	-	1	-
Rhaphoneis amphiceros		-	-	-	-	1	2	1	2
Rhaphoneis surirella		2	2	1	-	3	1	1	1
Surirella comis		1	-	-	-	-	-	-	-
Thalassionema nitzschiodes		1	-	-	-	2	-	-	-
Trachyneis aspera		1	-	1	-	-	1	-	-
Polyhalobous to Mesohalobous									
Actinoptychus undulatus		1	1	1	1	2	1	2	2
Cocconeis scutellum		-	1	1	-	-	-	-	-
Diploneis stroemii		-	-	-	-	-	-	1	-
Synedra gaillonii		-	-	-	-	-	1	-	-
Mesohalobous									
Achnanthes brevipes		-	1	-	-	-	-	-	-
Caloneis westii		1	-	1	-	-	-	2	1
Cyclotella striata		1	-	1	-	-	-	-	-
Diploneis didyma		1	1	-	1	-	-	-	1
Nitzschia punctata		1	-	2	-	-	1	-	-
Nitzschia granulata		-	1	-	-	-	-	1	-
Nitzschia hungarica		1	-	1	-	-	-	-	-
Nitzschia navicularis		1	1	-	-	1	1	-	1
Nitzschia sigma		-	1	-	-	1	-	-	-
Rhopalodia musculus		-	-	cf	-	cf	-	-	-
Scoliopleura brunksiensis		1	-	-	-	-	-	-	-
Scoliopleura tumida		1	1	1	1	-	2	1	1
Synedra tabulata		1	-	1	1	-	-	1	-
Mesohalobous to Halophil									
Actinocyclus normanii		-	-	1	-	-	-	-	-
Unknown Salinity Group									
Surirella sp.		-	-	-	-	1	-	-	-
Indet centric diatom		1	1	1	-	1	1	1	1
Indet pennate diatom		-	-	-	-	1	-	-	1
Indet. Naviculaceae		1	-	-	-	1	1	-	1
Cyclotella sp.		-	-	-	-	1	-	-	-
Diploneis sp.		-	-	-	-	1	-	1	-
Nitzschia sp.		1	-	1	-	-	-	-	-
Opephora sp.		1	-	-	-	-	-	-	-
Gyrosigma sp.		-	-	1	-	-	1	-	-
Navicula sp.		-	-	1	-	-	-	-	1
Synedra sp.		1	-	-	-	-	-	-	-
Thalassiosira sp.		-	-	-	-	1	-	-	-

5.4.3 The diatom assemblages of all eight samples are comprised of marine, marine-brackish and brackish-marine diatom species. Freshwater and halophilous diatoms are absent from the **VC_04** sequence.

5.5 Foraminifera and ostracods

5.5.1 Foraminifera occurred in all samples (**Table 8**), consisting of a few brackish calcareous species characteristic of low to mid saltmarsh; these foraminifera are of a very small size indicative of very low salinity. Throughout there were also small quantities of agglutinating foraminifera of one species (*Jadammina macrescens*), a detritivore on decaying plant material characteristic of high-mid saltmarsh.

5.5.2 Brackish ostracods were also present, although never in quantities of more than one or two in any sample, and often poorly preserved. There is clearly some decalcification, a process which ostracod are far more susceptible to than foraminifera, most likely occurring as a result of weathering of tidal flats. There are also a few very foraminifera and ostracods characteristic of outer estuarine that are likely to have drifted in on highest tides. Overall the assemblage is characteristic of brackish saltmarsh and mudflats.

Table 8 Results of foraminifera and ostracod assessment.

Taxon	Depth (mbsb)	2.51	2.64	2.75	2.87	2.97	3.32	3.44	3.56
BRACKISH FORAMINIFERA (calcareous foraminifera of low-mid saltmarsh and tidal flats)									
Haynesina germanica		x	x	xx	xx	x	xx	x	x
Ammoniasp. (brackish)		x	x	x	x	x	o	o	x
Elphidium williamsoni		-	o	x	x	x	x	-	o
Quinqueloculinasp. (brown)		-	o	-	o	-	-	-	-
(agglutinating foraminifera of mid-high saltmarsh)									
Jadammina macrescens		o	x	x	x	x	x	x	x
BRACKISH OSTRACODS (brackish ostracods of tidal flats and creeks)									
Leptocythere psammophila		x	o		x	o	o	-	o
Loxoconcha elliptica		-	o	o	-	-	o	-	o
Xestoleberis nitida		-	-	-	-	o	-	-	-
Cytherura gibba		-	-	-	-	o	-	-	-
OUTER ESTUARINE/MARINE FORAMINIFERA									
Lagenids		-	o	o	o	-	o	-	x
OUTER ESTUARINE/MARINE OSTRACODS									
Hirschmannia viridis		-	-	x	-	-	o	-	o

Foraminifera and ostracods are recorded: o – one specimen; x - several specimens; xx – common.

6 DISCUSSION

6.1 Introduction

6.1.1 The results of palaeoenvironmental assessment on vibrocore **VC_04** and OSL dating is discussed below, with consideration to how the data addresses the aims and objectives raised in **Section 2**, with recommendations made for further analysis (**Section 7**).

6.2 Sediments and chronology

Vibrocore VC_04

6.2.1 The two radiocarbon dates from the base and top of vibrocore **VC_04** (**Table 4**) produced dates of 14075-13771 (2.52-.2.54mbsb) and 13762-13484 cal. BP (3.56-3.58mbsb) respectively, corresponding with the Allerød interstadial (13.9-12.9ka). However, not only are the dates inverted, but they are significantly earlier than suggested by the pollen data from vibrocore **VC_04**, comprising pollen of thermophilous trees such as *Tilia* (lime) which are unequivocally characteristic of the Holocene and unlikely to have been present in this area much before approximately 8000 BP (Brewer et al 2017).

6.2.2 The difference between radiocarbon and pollen-derived dates of approximately 5500-6000 years is too great to derive solely from a marine reservoir effect, which is in the region of 400 years for the North Sea. It is more likely therefore that the radiocarbon dates are derived on material of Allerød interstadial date eroded into the channel.

Borehole BH-A03a

6.2.3 The quartz OSL and K-feldspar IRSL dates from a depth of 7.50 mbsf in **BH-A03a** range between 45.7 ± 4.7 and 38.9 ± 7.6 ka which is significantly (350 ka) younger than anticipated if the deposits are Hoxnian in age as predicted.

6.2.4 After reviewing the geotechnical log, deposits between 6.65 mbsf and 9.56 mbsf are characterised by very dense clayey fine sand which was initially interpreted to be part of the Egmond Ground Formation or Sand Hole Formation expected to have been deposited in a shallow marine to lagoonal environment during the Hoxnian (MIS 11) interglacial. The new optical dating results suggest these deposits were last exposed to light during the early parts of the last glacial period (MIS 3; Weichselian). If bleaching of the luminescence signal occurred during deposition of these deposits (apposed to post-deposition through a later phase of subaerial exposure), they are more likely related to the lower parts of Bolder Bank Formation which was deposited during the last ice age (Weichselian).

6.2.5 If this is the case, the sandy nature of these deposits may reflect deposition in front of an ice margin in a terrestrial, but cold and harsh, environment. There is a bed of high strength clay (glacial till) below the OSL sample at depths between 9.56 mbsf and 11.15 mbsf which supports the interpretation that these deposits were lain down in an ice-marginal environment. Ice is not expected to have reached the area of the TKOWF until sometime after 30 ka (Roberts et al 2018). However, these predictions are based on limited chronological information, based on the results presented here, ice may have reached the area earlier than previously predicted.

6.2.6 The archaeological potential of these deposits is expected to be low given they were deposited in an ice-marginal environment. However, of interest is these deposits are of a similar age to those located in Area 240 offshore of Norfolk where a rich and diverse assemblage of worked lithics and faunal remains were discovered (Tizzard et al 2015). These OSL ages can therefore be used to support regional palaeogeographic reconstructions.

6.2.7 The quartz OSL and K-feldspar IRSL dates from a depth of 26.05 mbsf range from 152.2 ± 20.0 ka to 361.8 ± 35.6 ka and are Saalian (MIS 6-10) in age, and these too are younger than expected. The age and lithology of these deposits show characteristics of Tea Hole Kettle Formation which has not been previously mapped within the TKOWF due to its sporadic and thin distribution across the southern North Sea (Cameron et al. 1992; WA 2017; Fugro 2016d).

6.2.8 The Saalian is a glacial period but it differs somewhat to the preceding Elsterian (MIS 12) and subsequent Weichselain (MIS 2) glacial periods as it apparently includes up to three periods of glaciation (MIS 10, MIS 8 and MIS 6), separated by two interglacial periods (MIS 9 and MIS 7). The timing of these glaciations differs across Europe making it difficult to correlate stratigraphic records.

6.2.9 In the UK sector of the southern North Sea, Saalian ice margins are not expected to have extended as far south as the TKOWF (Graham et al. 2011). Therefore, during periods of lower sea level, the area is likely to have been sub-aerially exposed. The Tea Kettle Hole Formation formed through cold-climate aeolian (wind) processes during these periods of exposure.

6.2.10 The British archaeological record during the Lower Palaeolithic is poorly understood but there is evidence of hominin activity in Britain (Lewis et al. 2011). Of particular interest, at Welton-Le-Wold in Lincolnshire, Lower Palaeolithic artefacts and Pleistocene faunal remains have been recovered from fluvial deposits overlain by till (Straw 1977, Bridgland et al. 2014). The stratigraphic context of this site shows similarities with the sequence recovered in **BH-03a**, although it is not known if the deposits dated at 26.05 mbsf are from a fluvial or aeolian setting, and they are also located ~60 km apart. Irrespective, the deposits have archaeological potential as they are interpreted to be deposited in an emergent southern North Sea during the Late Upper Palaeolithic.

6.2.11 The dating strategy used in **BH-03a** is relatively novel as it employed both quartz and K-feldspar dating techniques in an attempt to provide a reliable age estimate for deposits interpreted to be Holstenian in age (MIS 11; 424-374 ka). No previous attempts have been made to date Holstenian age deposits from the North Sea as they are considered to be beyond the maximum age limit of routine quartz OSL dating. Therefore, one of the key research questions driving this study was defined as follows;

- Are quartz OSL and K-feldspar Infrared Stimulated Luminescence (IRSL) viable techniques for dating deposits of Holsteinian age?

6.2.12 Over the last two decades, quartz has been the preferred mineral for luminescence dating as it is relatively stable when compared to feldspar. However, dating of deposits older than ~100 ka using quartz OSL is limited by the saturation of the quartz signal (Wintle and Murray 2006). In comparison, feldspar grains saturate at a much higher dose which means they have the potential to extend the upper age range of the luminescence technique. However, this approach was previously limited by an effect called “anomalous fading” which makes the luminescence signal unstable often leading to significant age underestimation (Wintle 1973). Recent advances in analytical techniques now allow for correction of anomalous fading (Buylaert et al. 2012; Li and Li 2011), providing a reliable method to date sediments much older than was previously possible using quartz OSL.

6.2.13 In terms of addressing the research question defined above, the optical dating results indicate the deposits are much younger than expected. Therefore, we are unable to test if the technique is viable for dating older Holstenian age sediments and we cannot answer this question explicitly.

6.2.14 However, the use of paired quartz OSL and K-feldspar IRSL dating was successful in improving our confidence in age estimates, despite analytical uncertainty driven by individual sample behaviour (see section **5.2**). For example, if we take the quartz OSL age from the sample at 7.50 mbsf, an age of 38.9 ± 7.6 ka was given, but this age can only be accepted as a minimum age estimate (i.e. true age is likely older than the given age) due

to significant feldspar contamination. Therefore, based on the quartz OSL date alone, there is potential the deposit could be Holstenian in age.

6.2.15 The K-feldspar date from the same sample depth (7.50 mbsf) returned and age of 45.7 ± 4.7 ka. However, due to failed dose recovery test, this age was accepted as a maximum age estimate (i.e. the true age is likely younger than the returned age). By using both techniques in parallel, we provided an age range for the deposit which indicates it is not in fact Holstenian age as expected.

6.2.16 There is therefore a lot of promise in using paired quartz OSL and K-feldspar dating strategies, especially where sample behaviour is less than perfect, as is proving to be the case when dating Middle Pleistocene deposits from the North Sea. By adopting this methodology, we can at least provide an age range for a deposit with a degree of confidence, which in an area where chronology is severely lacking, is a highly valuable contribution to our understanding of the deposits and their environmental history.

6.3 Palaeoenvironment (vibrocore VC_04)

6.3.1 The diatom assemblage from vibrocore **VC_04** is characteristic of marine, marine-brackish and brackish environments, with the foraminifera and ostracods assemblage characteristic of brackish saltmarsh and mudflats. There are no indications of freshwater influence.

6.3.2 The pollen provides an indication of the vegetation growing within both the wetland and adjoining dry ground environments. The dry ground is characterised by mix broadleaved woodland dominated oak-elm-lime and hazel. Alder, willow and birch will have formed components of the wetland flora, for example, alder-dominated fen carr woodland growing on wetter soils along the edges of channels. Pollen of Chenopodiaceae is present throughout the sequence indicating the nearby presence of saltmarsh consistent with the results of foraminiferal and ostracod assessment.

6.3.3 Together the results are consistent with a coastal brackish-marine environment of mudflats and saltmarsh dissected by tidal channels, but with areas of nearby dry ground supporting mature mixed deciduous woodland characteristic of the Holocene climatic optimum.

7 RECOMMENDATIONS

7.1.1 Based on the results of the palaeoenvironmental assessment and chronological information presented here, the geoarchaeological potential of deposits assessed, and potential for further Stage 4 targeted palaeoenvironmental analysis, is discussed below as discussed below and itemised in **Table 9**.

7.2 Saalian

7.2.1 A 12 m thick deposit of sand with beds of clay and black staining was recovered in **BH-03a**. Its location between Swarte Bank Formation till (MIS 12) and Bolder Bank Formation till (MIS 3-2) meant this deposit was interpreted as being Holstenian in age, belonging to the Sand Hole Formation (WA 2018). The results from paired K-feldspar IRSL and quartz OSL dating suggest this deposit formed between 152.2 ± 20.0 ka to 361.8 ± 35.6 ka which is earlier than expected as they are Saalian (MIS 6-10) in age.

7.2.2 These deposits have archaeological potential as they were deposited in an emergent southern North Sea during the Late Lower Palaeolithic; a period with a sparse but known archaeological record in Britain. However, the coarse-grained nature of sediments means the potential for preservation of palaeoenvironmental material is low, and the likelihood of

encountering artefactual material within a borehole sample is low. Therefore, no further geoarchaeological work is recommended.

Table 9 Potential of existing samples for analysis, vibrocore **VC_04**.

Sample depth (mbsb)	Pollen			Diatom			Foraminifera Ostracods
	pres.	conc.	potential	pres.	conc.	potential	
2.52	2	1	G	4/3	4	M	n/a
2.64	2	1	G	4/3	4	M/L	
2.75	2	1	G	4/3	4	M	
2.87	2	1	G	4	5	L	
2.97	2	1	G	4	5	L	
3.32	2	1	G	4/3	4	M/L	
3.44	2	1	G	4	4	L	
3.56	2	1	G	4/3	4	M	

Preservation and concentration: 1=excellent, 2=good, 3=moderate, 4=poor, 5=very poor. Potential: G=good, M=moderate, L=low, N=none.

7.3 Early Weichselain

7.3.1 Lower Bolders Bank (**Unit 5**) was dated using paired K-feldspar IRSL and quartz OSL dating in **BH-03a**. The geoarchaeological potential of these deposits is expected to be low given they were deposited in an ice-marginal environment. Therefore, no further work is recommended.

7.4 Early Holocene

7.4.1 The geoarchaeological potential of Early Holocene deposits (**Unit 6**) in vibrocore **VC_04** is itemised in **Table 9** detailing the potential to progress the current assessment-level data through to full analysis.

Pollen

7.4.2 Vibrocore **VC_04** has excellent preservation and concentration of pollen grains and therefore holds potential for Stage 4 palaeoenvironmental analysis. However, any further Stage 4 analysis would need to be considered alongside a robust chronological framework and the minerogenic rich deposits recovered in **VC-04** present significant difficulties for radiocarbon dating. No plant macrofossils are preserved and the two radiocarbon dates on bulk sediment are inverted (i.e. not in stratigraphic order). Furthermore, the results produce significantly earlier dates than indicated by pollen results. Uncertainty around the radiocarbon dates and a lack of suitable material for further dating limits the potential of these deposits for Stage 4 analysis. Moreover, there is little apparent change in the overall pollen signal within the deposits and Stage 4 analysis will unlikely add any additional information than already presented during the Stage 3 assessment. Therefore, no further pollen analysis is recommended.

Diatoms

7.4.3 Diatoms are present in all eight samples from vibrocore **VC_04**, but the concentrations are generally low and preservation varying from very poor to poor and moderate. The potential for further analysis is moderate-low in five sub-samples and low in three sub-samples (**Table 8**). No further diatom analysis is recommended.

Foraminifera and ostracod

7.4.4 The current foraminifera/ostracod assessments are considered sufficient and no further analysis of these remains is recommended from vibrocore **VC-04**.

BIBLIOGRAPHY

Adamiec, G and Aitken, M J 1998 Dose-rate conversion factors: new data. *Ancient TL*, 16, 37-50

Athersuch, J, Horne, D J and Whittaker, J E 1989 Marine and Brackish Water Ostracods. Leiden, Brill

Battarbee, R W, Jones, V J, Flower, R J, Cameron, N G, Bennion, H B, Carvalho, L and Juggins, S 2001 Diatoms, in J P Smol and H J B. Birks (eds) *Tracking Environmental Change Using Lake Sediments Volume 3: terrestrial, algal, and siliceous indicators*, 155–202. Dordrecht, Kluwer Academic Publishers

Bennett, K D, Whittington, G and Edwards, K J 1994 Recent plant nomenclatural changes and pollen morphology in the British Isles, *Quat Newsl* 73, 1–6

Brewer, S, Giesecke, T, Davis, B A S, Finsinger, W, Wolters, S, Binney, H, de Beaulieu, J-L, Fyfe, R, Gil-Romera, G, Kuhl, N, Kunes, P, Leydet, M and Bradshaw, R H 2017 Late glacial and Holocene European pollen data, *J Maps* 13, 921–928

Bridgland D.R. Howard A.J. White M.J. and White T.S. 2014 Quaternary of the Trent. Oxbow Books: Oxford. 406 pp.

Bronk Ramsey, C and Lee, S 2013 Recent and planned development of the Program OxCal, *Radiocarbon* 55(2-3), 720–730

Cameron, T D J, Crosby, A, Balson, P S, Jeffery, D H , Lott, G K, Bulat, J and Harrison, D J 1992 *The Geology of the Southern North Sea*. London HMSO, British Geological Survey United Kingdom Offshore Report

Cushing, E J 1967 Evidence for differential pollen preservation in late Quaternary sediments in Minnesota, *Rev of Palaeobotany Palynol* 4, 87–101

Flower, R J 1993 Diatom preservation: experiments and observations on dissolution and breakage in modern and fossil material. *Hydrobiologia 269/270*, 473–484

Fugro GeoConsulting Ltd 2009 *Geotechnical Report: Triton Knoll Offshore Wind Farm Geotechnical Site Investigation*. Wallingford, unpubl report ref: 20911026-3

Fugro Geoconsulting Ltd 2016d *Triton Knoll Offshore Wind Farm Limited, Ground Model Technical Report for Foundations*. Wallingford, unpubl rep J31134-R-001(03)

Fugro Geoconsulting Ltd 2016e *Triton Knoll Offshore Wind Farm Limited, Ground Model Technical Report for Array Cables*. Wallingford, unpubl rep J31134-R-003(02)

Fugro Geoconsulting Ltd 2016f *Triton Knoll Offshore Wind Farm Limited, Ground Model Technical Report for Export Cables*. Wallingford, unpubl rep J31134-R-004(03)

Graham, A G C, Stoker, M S, Lonergan, L, Bradwell, T and Stewart, M 2011 The Pleistocene Glaciations of the North Sea Basin. In: Ehlers, J and Gibbard, P L and Hughes, P D (eds) *Quaternary Glaciations – Extent and Chronology: A Closer Look*. Vol. 15, 2-1108, Amsterdam, Netherlands, Elsevier.

Hartley, B, Barber, H G, Carter J R and Sims, P A 1996 *An Atlas of British Diatoms.* Bristol, Biopress Ltd

Hendey, N I 1964 *An Introductory Account of the Smaller Algae of British Coastal Waters, Part V. Bacillariophyceae (Diatoms).* Ministry of Agriculture Fisheries and Food, Series IV

Hustedt, F 1953 Die Systematik der Diatomeen in ihren Beziehungen zur Geologie und Okologienebst einer Revision des Halobien-systems, *Sv Bot Tidskr* 47, 509–519

Hustedt, F 1957 Die Diatomeenflora des Fluss-systems der Weser im Gebiet der Hansestadt Bremen, *Ab Naturw Ver Bremen* 34, 181–440

Krammer, K and Lange-Bertalot, H 1986-1991 *Bacillariophyceae.* Stuttgart*,* Gustav Fisher Verlag

Lewis S G, Ashton N and Jacobi, R 2011 Testing Human Presence during the Last Interglacial (MIS 5e): A Review of the British Evidence, in Ashton N, Lewis, S G, and Stringer, C (eds.) *The Ancient Human Occupation of Britain*. Vol.14, 125-247, Amsterdam, Netherlands, Elsevier

Li, B, Roberts, R G, Jacobs, Z and Li, S-H 2014 A single-aliquot luminescence dating procedure for K-feldpsar based on the dose-dependent MET-pIRIR signal sensitivity. *Quat Geochron*, 20, 51-64.

Meisch, C 2000 *Freshwater Ostracoda of Western and Central Europe*. (Suβwasserfauna von Mitteleuropa, Band 8/3). Berlin, Spektrum Akadamischer Verlag

Mejdahl, V 1979 Thermoluminescence dating: beta-dose attenuation in quartz grains. A*rchaeometry*, 21, 61-72

Moore, P D, Webb, J A. and Collinson, M E 1991 *Pollen analysis* (2nd edition). Oxford, Blackwell

Murray, J W 2006 *Ecology and Applications of Benthic Foraminifera.* Cambridge, Cambridge University Press

Murray, A S and Wintle, A G 2000 Luminescence dating of quartz using an improved single-aliquot regenerative-dose protocol. *Radiation Measurements*, 32, 57-73

Murray, A S and Wintle, A.G 2003 The single aliquot regenerative dose protocol: potential for improvements in reliability. *Radiation Measurements*, 37, 377-381

Prescott, J R and Hutton, J T 1994 Cosmic ray contributions to dose rates for luminescence and ESR dating: large depths and long-term time variations. *Radiation Measurements*, 23, 497-500

Reimer, P J, Bard, E, Bayliss, A, Beck, J W, Blackwell, P G, Bronk Ramsey, C, Grootes, P M, Guilderson, T P, Haflidason, H, Hajdas, I, HattŽ, C, Heaton, T J, Hoffmann, D L, Hogg, A G, Hughen, K A, Kaiser, K F, Kromer, B, Manning, S W, Niu, M, Reimer, R W, Richards, D A, Scott, E M, Southon, J R, Staff, R A, Turney, C S M and van der Plicht, J 2013 IntCal13 and Marine13 Radiocarbon Age Calibration Curves 0-50,000 Years cal BP, *Radiocarbon* 55(4), 1869–1887

Roberts, D H, Evans, D J A, Callard, S L, Clarke, C D, Bateman, M D, Medialdea, A, Dove, D, Cotterill, C J, Saher, M, Cofaigh, C O, Chiverrell, R C, Moreton, S G, Fabel, D and Bradwell, T 2018 Ice marginal dynamics of the last British-Irish Ice Sheet in the southern North Sea: Ice limits, timing and the influence of Dogger Bank *Quat Sci Rev* 198, 181-207

Royal HaskoningDHV 2016a *Triton Knoll Offshore Wind Farm Limited Archaeological Written Scheme of Investigation (Offshore)*, unpubl report ref. 2505-TKN-HOS-G-RA-0001

Royal HaskoningDHV 2016b *Triton Knoll Offshore Wind Farm Limited Archaeological Method Statement: Offshore Geotechnical Site Investigations*, unpubl report ref. *2505-TKN-HOS-G-SM-0001-01*

Ryves, D B, Juggins, S, Fritz, S C. and Battarbee, R W 2001 Experimental diatom dissolution and the quantification of microfossil preservation in sediments, *Palaeogeog Palaeoclimatol Palaeoecol* 172, 99–113

Stace, C 1997 *New flora of the British Isles* (2nd edition), Cambridge, Cambridge University Press

Tizzard, L, Bicket, A. R, Benjamin, J and De Loecker, D 2015 *A Middle Palaeolithic Site in the Southern North Sea: Investigating the Archaeology and Palaeogeography of Area 240*. Salisbury, Wessex Archaeology Monograph no 35

Straw A. 1977 Welton-le-Wold. In: J.A, Catt (ed) *Yorkshire and Lincolnshire Field Guidebook for Excursion C7*. Tenth INQUA Congress, Birmingham, Geo. Abstracts, Notrwich, 21-23.

Wessex Archaeology 2009 *Geoarchaeology: note on cores.* Salisbury, unpubl rep 70070

Wessex Archaeology 2011 *Triton Knoll Offshore Wind Farm: desk-based archaeological assessment*. Salisbury, unpubl rep 70070.09

Wessex Archaeology 2010 *Triton Knoll Offshore Wind Farm: stage 2 geoarchaeological recording of borehole samples*. Salisbury, unpubl rep 70070.01

Wessex Archaeology 2015 Triton Knoll Offshore Wind Farm: written scheme of investigation for geotechnical survey. Salisbury, unpubl rep 70075.01

Wessex Archaeology 2016a *Triton Knoll Offshore Wind Farm: stage 1 geoarchaeological assessment of geotechnical logs*. Salisbury, unpubl rep 70076.04

Wessex Archaeology 2016b *Triton Knoll Offshore Wind Farm and Export Cable Corridor: stage 1 archaeological assessment of 2016 geotechnical logs*. Salisbury, unpubl rep 70076.05

Wessex Archaeology 2017 *Triton Knoll Offshore Wind Farm and Export Cable Route: archaeological assessment of geophysical data*. Salisbury, unpubl rep 70076.03

Wessex Archaeology 2018 *Triton Knoll Offshore Wind Farm and Export Cable Corridor: stage 2 geoarchaeological recording of geotechnical samples.* Salisbury, unpubl rep 70076.06

Witkowski, A, Lange-Bertalot, H and Metzeltin, D 2000 *Diatom Flora of Marine Coasts I.* Iconographia Diatomologica Volume 7. Königstein, A.R.G. Gantner Verlag Koeltz Scientific Books

Van Der Werff, A and Huls, H 1957-1974 *Diatomeenflora van Nederland*, 10 volumes

Zimmerman, D W 1971 Thermoluminescent dating using fine grains from pottery. *Archaeometry*, 13, 29-52

APPENDECES

Appendix 1 - Figures

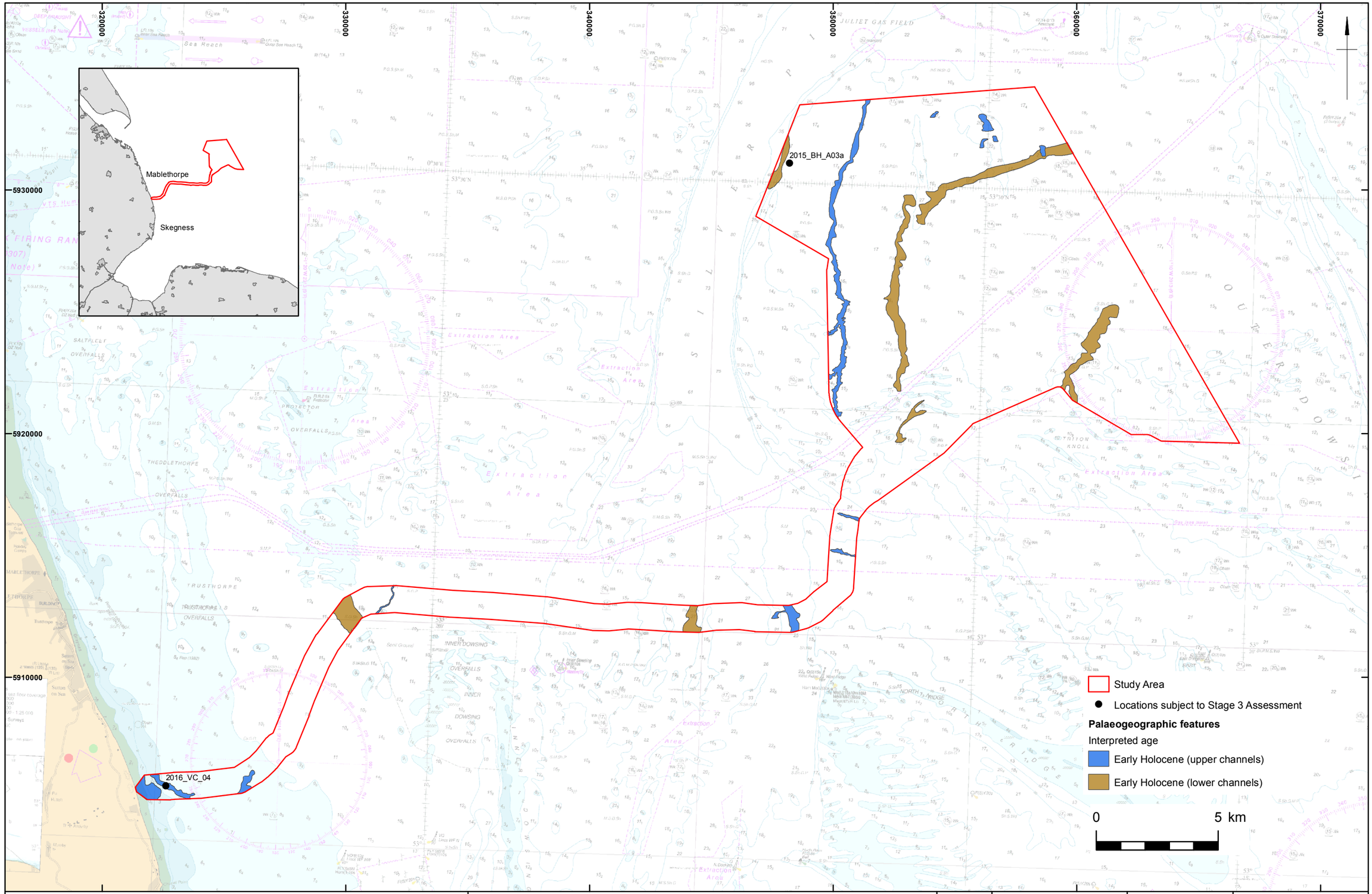

Date:	27/09/2018	Revision Number:	0
Scale:	1:150,000 at A3	Illustrator:	KJF
Path:	W\Projects\70076\GIS\FigsMXD\Geoarch_Stage3_Sept2018		

Geotechnical sample locations

Figure 1

Appendix 2 - OSL Reports

University of Gloucestershire

Luminescence dating laboratory

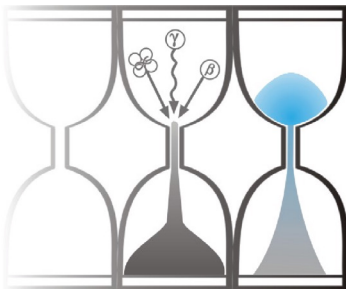

Paired Quartz & K-Feldspar Optical dating of sediments: Triton Knoll Borehole, UK

to

Dr A. Brown and Dr C. Mellett

Wessex Archaeology

Analysis & Reporting, Dr P.S. Toms
Sample Preparation & Measurement, Mr J.C. Wood
12 September 2018

Contents

Scope of Report

This is a standard report of the Luminescence dating laboratory, University of Gloucestershire. In large part, the document summarises the processes, diagnostics and data drawn upon to deliver Table 1. A conclusion on the analytical validity of each sample's optical age estimate is expressed in Table 2; where there are caveats, the reader is directed to the relevant section of the report that explains the issue further in general terms.

Copyright Notice

Field Code	Lab Code	Overburden (m)	Grain size (μm)	Moisture content (%)	NaI γ-spectrometry (*in situ*) γ D_r ($Gy.ka^{-1}$)	Ge γ-spectrometry (*ex situ*)			Internal β D_r ($Gy.ka^{-1}$)	External β D_r ($Gy.ka^{-1}$)	External γ D_r ($Gy.ka^{-1}$)	Cosmic D_r ($Gy.ka^{-1}$)	Preheat (°C for 10s)	Low Dose Repeat Ratio	High Dose Repeat Ratio	Post-IR OSL Ratio
						K (%)	Th (ppm)	U (ppm)								
BHA03a – 7.50 m	GL17150 Quartz	7.6	125-180	19 ± 5	-	1.29 ± 0.09	4.34 ± 0.40	1.09 ± 0.12	-	0.92 ± 0.12	0.51 ± 0.09	0.07 ± 0.01	260	1.00 ± 0.03	1.03 ± 0.03	0.81 ± 0.02
	GL17150 K-Feldspar								0.57 ± 0.11				-	1.01 ± 0.02	0.98 ± 0.02	-

Field Code	Lab Code	Total D_r ($Gy.ka^{-1}$)	D_e (Gy)	Age (ka)
BHA03a – 7.50 m	GL17150 Quartz	1.50 ± 0.15	58.3 ± 9.6	38.9 ± 7.6 (7.3)
	GL17150 K-Feldspar	2.07 ± 0.18	94.3 ± 4.9	45.7 ± 4.7 (4.2)

Table 1 D_r, D_e and Age data of submitted samples located at c. 53°N, 1°E, 0m. Age estimates expressed relative to year of sampling. Uncertainties in age are quoted at 1σ confidence, are based on analytical errors and reflect combined systematic and experimental variability and (in parenthesis) experimental variability alone (see 6.0). **Blue** indicates samples with accepted age estimates, **red**, age estimates with caveats (see Table 2).

Generic considerations	Field Code	Lab Code	Sample specific considerations
Absence of *in situ* γ spectrometry data (see section 4.0)	BHA03a – 7.50 m	GL17150 Quartz	Significant feldspar contamination (see section 3.1.1, Table 1 and Fig. 1) Accept as minimum age estimate
		GL17150 K-Feldspar	Failed Dose Recovery test (see section 3.1.2 and Fig. 2) Accept as maximum age estimate

Table 2 Analytical validity of sample suite age estimates and caveats for consideration

1.0 Mechanisms and principles

Upon exposure to ionising radiation, electrons within the crystal lattice of insulating minerals are displaced from their atomic orbits. Whilst this dislocation is momentary for most electrons, a portion of charge is redistributed to meta-stable sites (traps) within the crystal lattice. In the absence of significant optical and thermal stimuli, this charge can be stored for extensive periods. The quantity of charge relocation and storage relates to the magnitude and period of irradiation. When the lattice is optically or thermally stimulated, charge is evicted from traps and may return to a vacant orbit position (hole). Upon recombination with a hole, an electron's energy can be dissipated in the form of light generating crystal luminescence providing a measure of dose absorption.

In this report, both quartz and K-feldspar were segregated for dating. The utility of quartz as a minerogenic dosimeter lies in the stability of its datable signal over the mid to late Quaternary period, predicted through isothermal decay studies (e.g. Smith *et al*., 1990; retention lifetime 630 Ma at 20°C) and evidenced by optical age estimates concordant with independent chronological controls (e.g. Murray and Olley, 2002). This stability is in contrast to the anomalous fading of comparable signals commonly observed for other ubiquitous sedimentary minerals such as feldspar and zircon (Wintle, 1973; Templer, 1985; Spooner, 1993). However, recent studies of K-feldspar have identified a non-fading signal (Thomsen et al., 2008). And with the ability of feldspar to accumulate signal over periods longer than that of quartz, paired quartz and K-feldspar dating is a pragmatic approach for samples that may date earlier than the Late Pleistocene.

Optical age estimates of sedimentation (Huntley *et al*., 1985) are premised upon reduction of the minerogenic time dependent signal (Optically Stimulated Luminescence, OSL) to zero through exposure to sunlight and, once buried, signal reformulation by absorption of litho- and cosmogenic radiation. The signal accumulated post burial acts as a dosimeter recording total dose absorption, converting to a chronometer by estimating the rate of dose absorption quantified through the assay of radioactivity in the surrounding lithology and streaming from the cosmos.

$$\text{Age} = \frac{\text{Mean Equivalent Dose } (D_e, \text{ Gy})}{\text{Mean Dose Rate } (D_r, \text{ Gy.ka}^{-1})}$$

Aitken (1998) and Bøtter-Jensen *et al*. (2003) offer a detailed review of optical dating.

2.0 Sample Preparation

One sediment core was collected within opaque tubing and submitted for Optical dating. To preclude optical erosion of the datable signal prior to measurement, the sample was opened and prepared under controlled laboratory illumination provided by Encapsulite RB-10 (red) filters. To isolate that material potentially exposed to daylight during sampling, sediment located within 10 mm of each core face was removed.

The remaining sample was dried and then sieved. The fine sand fraction was segregated and subjected to acid and alkaline digestion (10% HCl, 15% H_2O_2) to attain removal of carbonate and organic components respectively. The sample was then divided in two. For one half, a further acid digestion in HF (40%, 60 mins) was used to etch the outer 10-15 μm layer affected by α radiation and degrade each samples' feldspar content. During HF treatment, continuous magnetic stirring was used to effect isotropic etching of grains. 10% HCl was then added to remove acid soluble fluorides. Each sample was dried, resieved and quartz isolated from the remaining heavy mineral fraction using a sodium polytungstate density separation at 2.68g.cm^{-3}. For the second half, density separations at 2.53 and 2.58 g cm^{-3} were undertaken to isolate the K-feldspar fraction. Twelve 8 mm multi-grain aliquots (*c*. 3-6 mg) of quartz and K-feldspar were then mounted on aluminium discs for determination of D_e values.

All drying was conducted at 40°C to prevent thermal erosion of the signal. All acids and alkalis were Analar grade. All dilutions (removing toxic-corrosive and non-minerogenic luminescence-bearing substances) were conducted with distilled water to prevent signal contamination by extraneous particles.

3.0 Acquisition and accuracy of D_e value

All minerals naturally exhibit marked inter-sample variability in luminescence per unit dose (sensitivity). Therefore, the estimation of D_e acquired since burial requires calibration of the natural signal using known amounts of laboratory dose. D_e values were quantified using a single-aliquot regenerative-dose (SAR) protocol (Murray and Wintle 2000, 2003 for quartz; Li et al., 2014 for K-feldspar) facilitated by a Risø TL-DA-15 irradiation-stimulation-detection system (Markey *et al*., 1997; Bøtter-Jensen *et al*., 1999). Within this apparatus, optical signal stimulation of quartz is provided by an assembly of blue diodes (5 packs of 6 Nichia NSPB500S), filtered to 470±80 nm conveying 15 $mW.cm^{-2}$ using a 3 mm Schott GG420 positioned in front of each diode pack. Infrared (IR) stimulation for K-feldspars is provided by 6 IR diodes (Telefunken TSHA 6203) stimulating at 875±80nm delivering ~5 $mW.cm^{-2}$. Stimulated photon emissions from quartz aliquots are in the ultraviolet (UV) range and were filtered from stimulating photons by 7.5 mm HOYA U-340 glass and detected by an EMI 9235QA photomultiplier fitted with a blue-green sensitive bialkali photocathode. K-feldpar emissions were filtered by 2 mm Schott BG-39 and 3mm Schott BG-3 glass. Aliquot irradiation was conducted using a 1.48 GBq $^{90}Sr/^{90}Y$ β source calibrated for multi-grain aliquots of 125-180 μm quartz and feldspar against the 'Hotspot 800' ^{60}Co γ source located at the National Physical Laboratory (NPL), UK.

SAR by definition evaluates D_e through measuring the natural signal (Fig. 1) of a single aliquot and then regenerating that aliquot's signal by using known laboratory doses to enable calibration. For each aliquot, five different regenerative-doses were administered so as to image dose response. D_e values for each aliquot were then interpolated, and associated counting and fitting errors calculated, by way of exponential plus linear regression (Fig. 1). Weighted (geometric) mean D_e values were calculated from 12 aliquots using the central age model outlined by Galbraith *et al*. (1999) and are quoted at 1σ confidence (Table 1). The accuracy with which D_e equates to total absorbed dose and that dose absorbed since burial was assessed. The former can be considered a function of laboratory factors, the latter, one of environmental issues. Diagnostics were deployed to estimate the influence of these factors and criteria instituted to optimise the accuracy of D_e values.

3.1 Laboratory Factors

3.1.1 Feldspar contamination of quartz

The propensity of feldspar signals to fade and underestimate age, coupled with their higher sensitivity relative to quartz makes it imperative to quantify feldspar contamination. At room temperature, feldspars generate a signal (IRSL; Fig. 1) upon exposure to IR whereas quartz does not. The signal from feldspars contributing to OSL can be depleted by prior exposure to IR. For all aliquots the contribution of any remaining feldspars was estimated from the OSL IR depletion ratio (Duller, 2003). The influence of IR depletion on the OSL signal can be illustrated by comparing the regenerated post-IR OSL D_e with the applied regenerative-dose. If the addition to OSL by feldspars is insignificant, then the repeat dose ratio of OSL to post-IR OSL should be statistically consistent with unity (Table 1). If any aliquots do not fulfil this criterion, then the sample age estimate should be accepted tentatively. The source of feldspar contamination is rarely rooted in sample preparation; it predominantly results from the occurrence of feldspars as inclusions within quartz.

3.1.2 Preheating

Preheating aliquots between irradiation and optical stimulation is necessary to ensure comparability between natural and laboratory-induced signals. However, the multiple irradiation and preheating steps that are required to define single-aliquot regenerative-dose response leads to signal sensitisation, rendering calibration of the natural signal inaccurate.

The SAR protocol (Murray and Wintle, 2000; 2003) enables this sensitisation to be monitored and corrected using a test dose to track signal sensitivity between irradiation-preheat steps. In the case of quartz a 5 Gy test dose preheated to 220°C for 10s was used. For K-feldspar a 30 Gy test dose and 300°C preheat for 60s was applied (Li et al. 2014), However, the accuracy of sensitisation correction for both natural and laboratory signals can be preheat dependent.

The Dose Recovery test was used to assess the optimal preheat temperature for accurate correction and calibration of the time dependent signal. Dose Recovery (Fig. 2) attempts to quantify the combined effects of thermal transfer and sensitisation on the natural signal, using a precise lab dose to simulate natural dose. The ratio between the applied dose and recovered D_e value should be statistically concordant with unity. For this diagnostic, in the case of quartz, 6 aliquots were each assigned a 10 s preheat between 180°C and 280°C. For the K-feldspar fraction, the efficacy of the 300°C, 60s preheat in Dose Recovery was assessed from the average of three aliquots.

That preheat treatment fulfilling the criterion of accuracy within the Dose Recovery test was selected to generate the final D_e value from a further 12 aliquots. Further thermal treatments, prescribed by Murray and Wintle (2000; 2003), were applied to optimise accuracy and precision. Optical stimulation of quartz occurred at 125ºC in order to minimise effects associated with photo-transferred thermoluminescence and maximise signal to noise ratios (Murray and Wintle, 2000; 2003). For K-feldspar, optical stimulation was performed at 50°C then 200°C to remove the fading signal, with the non-fading signal then measured at 250°C (Li et al., 2014). Inter-cycle optical stimulation was conducted at 280ºC for quartz and 320ºC for K-feldspar to minimise recuperation.

3.1.3 Internal consistency

Abanico plots (Dietze *et al*., 2016) are used to illustrate inter-aliquot D_e variability (Fig. 3). D_e values are standardised relative to the central D_e value for natural signals and are described as overdispersed when >5% lie beyond $\pm 2\sigma$ of the standardising value; resulting from a heterogeneous absorption of burial dose and/or response to the SAR protocol. For multi-grain aliquots, overdispersion of natural signals does not necessarily imply inaccuracy. However where overdispersion is observed for regenerated signals, the efficacy of sensitivity correction may be problematic. Murray and Wintle (2000; 2003) suggest repeat dose ratios (Table 1) offer a measure of SAR protocol success, whereby ratios ranging across 0.9-1.1 represent effective sensitivity correction. However, this variation of repeat dose ratios in the high-dose region can have a significant impact on D_e interpolation.

3.2 Environmental factors

3.2.1 Incomplete zeroing

Post-burial OSL signals residual of pre-burial dose absorption can result where pre-burial sunlight exposure is limited in spectrum, intensity and/or period, leading to age overestimation. This effect is particularly acute for material eroded and redeposited sub-aqueously (Olley *et al*., 1998, 1999; Wallinga, 2002) and exposed to a burial dose of <20 Gy (e.g. Olley *et al*., 2004), has some influence in sub-aerial contexts but is rarely of consequence where aerial transport has occurred. Within single-aliquot regenerative-dose optical dating there are two diagnostics of partial resetting (or bleaching); signal analysis (Agersnap-Larsen *et al*., 2000; Bailey *et al*., 2003) and inter-aliquot D_e distribution studies (Murray *et al*., 1995).

Within this stud signal analysis, which is only applicable to quartz, was used to quantify the change in D_e value with respect to optical stimulation time for multi-grain aliquots. This exploits the existence of traps within minerogenic dosimeters that bleach with different efficiency for a given wavelength of light to verify partial bleaching. D_e (t) plots (Fig. 4; Bailey *et al*., 2003) are constructed from separate integrals of signal decay as laboratory optical stimulation progresses. A statistically significant increase in natural D_e (t) is indicative of partial bleaching assuming three conditions are fulfilled. Firstly, that a statistically significant increase in D_e (t) is observed when partial bleaching is simulated within the laboratory. Secondly, that there is no significant rise in D_e (t) when full bleaching is simulated. Finally, there should be

no significant augmentation in D_e (t) when zero dose is simulated. Where partial bleaching is detected, the age derived from the sample should be considered a maximum estimate only. However, the utility of signal analysis is strongly dependent upon a samples pre-burial experience of sunlight's spectrum and its residual to post-burial signal ratio. Given in the majority of cases, the spectral exposure history of a deposit is uncertain, the absence of an increase in natural D_e (t) does not necessarily testify to the absence of partial bleaching.

Where requested and feasible, the insensitivities of multi-grain single-aliquot signal analysis may be circumvented by inter-aliquot D_e distribution studies, which can be attempted on both quartz and K-feldspars. This analysis uses aliquots of single sand grains to quantify inter-grain D_e distribution. At present, it is contended that asymmetric inter-grain D_e distributions are symptomatic of partial bleaching and/or pedoturbation (Murray *et al*., 1995; Olley *et al*., 1999; Olley *et al*., 2004; Bateman *et al*., 2003). For partial bleaching at least, it is further contended that the D_e acquired during burial is located in the minimum region of such ranges. The mean and breadth of this minimum region is the subject of current debate, as it is additionally influenced by heterogeneity in microdosimetry, variable inter-grain response to SAR, residual to post-burial signal ratios and, in the case of K-feldspar, inter-grain variations in K content.

3.2.2 Turbation

As noted in section 3.1.1, the accuracy of sedimentation ages can further be controlled by post-burial trans-strata grain movements forced by pedo- or cryoturbation. Berger (2003) contends pedogenesis prompts a reduction in the apparent sedimentation age of parent material through bioturbation and illuviation of younger material from above and/or by biological recycling and resetting of the datable signal of surface material. Berger (2003) proposes that the chronological products of this remobilisation are A-horizon age estimates reflecting the cessation of pedogenic activity, Bc/C-horizon ages delimiting the maximum age for the initiation of pedogenesis with estimates obtained from Bt-horizons providing an intermediate age 'close to the age of cessation of soil development'. Singhvi et al. (2001), in contrast, suggest that B and C-horizons closely approximate the age of the parent material, the A-horizon, that of the 'soil forming episode'. Recent analyses of inter-aliquot D_e distributions have reinforced this complexity of interpreting burial age from pedoturbated deposits (Lombard *et al*., 2011; Gliganic *et al*., 2015; Jacobs *et al*., 2008; Bateman *et al*., 2007; Gliganic *et al*., 2016). At present there is no definitive post-sampling mechanism for the direct detection of and correction for post-burial sediment remobilisation. However, intervals of palaeosol evolution can be delimited by a maximum age derived from parent material and a minimum age obtained from a unit overlying the palaeosol. Inaccuracy forced by cryoturbation may be bidirectional, heaving older material upwards or drawing younger material downwards into the level to be dated. Cryogenic deformation of matrix-supported material is, typically, visible; sampling of such cryogenically-disturbed sediments can be avoided.

4.0 Acquisition and accuracy of D_r value

For lithogenic radiation external to the grains of quartz and K-feldspar, D_r values were defined through measurement of U, Th and K radionuclide concentration and conversion of these quantities into β and γ D_r values (Table 1). β contributions were estimated from sub-samples by laboratory-based γ spectrometry using an Ortec GEM-S high purity Ge coaxial detector system, calibrated using certified reference materials supplied by CANMET. γ dose rates can be estimated from *in situ* NaI gamma spectrometry or, where direct measurements are unavailable as in the present case, from laboratory-based Ge γ spectrometry. *In situ* measurements reduce uncertainty relating to potential heterogeneity in the γ dose field surrounding each sample. The level of U disequilibrium was estimated by laboratory-based Ge γ spectrometry. Estimates of radionuclide concentration were converted into D_r values (Adamiec and Aitken, 1998), accounting for D_r modulation forced by grain size (Mejdahl, 1979) and present moisture content (Zimmerman, 1971). Lithogenic radiation internal to K-feldspar grains was assumed to be derived from a K content of 12.5%. Cosmogenic D_r

values were calculated on the basis of sample depth, geographical position and matrix density (Prescott and Hutton, 1994).

The spatiotemporal validity of D_r values can be considered a function of five variables. Firstly, age estimates devoid of *in situ* γ spectrometry data should be accepted tentatively if the sampled unit is heterogeneous in texture or if the sample is located within 300 mm of strata consisting of differing texture and/or mineralogy. However, where samples are obtained throughout a vertical profile, consistent values of γ D_r based solely on laboratory measurements may evidence the homogeneity of the γ field and hence accuracy of γ D_r values. Secondly, disequilibrium can force temporal instability in U and Th emissions. The impact of this infrequent phenomenon (Olley *et al*., 1996) upon age estimates is usually insignificant given their associated margins of error. However, for samples where this effect is pronounced (>50% disequilibrium between ^{238}U and ^{226}Ra; Fig. 5), the resulting age estimates should be accepted tentatively. Thirdly, pedogenically-induced variations in matrix composition of B and C-horizons, such as radionuclide and/or mineral remobilisation, may alter the rate of energy emission and/or absorption. If D_r is invariant through a dated profile and samples encompass primary parent material, then element mobility is likely limited in effect. Fourthly, spatiotemporal detractions from present moisture content are difficult to assess directly, requiring knowledge of the magnitude and timing of differing contents. However, the maximum influence of moisture content variations can be delimited by recalculating D_r for minimum (zero) and maximum (saturation) content. Finally, temporal alteration in the thickness of overburden alters cosmic D_r values. Cosmic D_r often forms a negligible portion of total D_r. It is possible to quantify the maximum influence of overburden flux by recalculating D_r for minimum (zero) and maximum (surface sample) cosmic D_r.

5.0 Estimation of Age

Ages reported in Table 1 provide an estimate of sediment burial period based on mean D_e and D_r values and their associated analytical uncertainties. Uncertainty in age estimates is reported as a product of systematic and experimental errors, with the magnitude of experimental errors alone shown in parenthesis (Table 1). Cumulative frequency plots indicate the inter-aliquot variability in age (Fig. 6). The maximum influence of temporal variations in D_r forced by minima-maxima in moisture content and overburden thickness is also illustrated in Fig. 6. Where uncertainty in these parameters exists this age range may prove instructive, however the combined extremes represented should not be construed as preferred age estimates. The analytical validity of each sample is presented in Table 2.

6.0 Analytical uncertainty

All errors are based upon analytical uncertainty and quoted at 1σ confidence. Error calculations account for the propagation of systematic and/or experimental (random) errors associated with D_e and D_r values.

For D_e values, systematic errors are confined to laboratory β source calibration. Uncertainty in this respect is that combined from the delivery of the calibrating γ dose (1.2%; NPL, pers. comm.), the conversion of this dose for SiO_2 using the respective mass energy-absorption coefficient (2%; Hubbell, 1982) and experimental error, totalling 3.5%. Mass attenuation and bremsstrahlung losses during γ dose delivery are considered negligible. Experimental errors relate to D_e interpolation using sensitisation corrected dose responses. Natural and regenerated sensitisation corrected dose points (S_i) were quantified by,

$$S_i = (D_i - x.L_i) / (d_i - x.L_i) \qquad \textbf{Eq.1}$$

where D_i = Natural or regenerated OSL, initial 0.2 s

L_i = Background natural or regenerated OSL, final 5 s

d_i = Test dose OSL, initial 0.2 s

x = Scaling factor, 0.08

The error on each signal parameter is based on counting statistics, reflected by the square-root of measured values. The propagation of these errors within Eq. 1 generating σS_i follows the general formula given in Eq. 2. σS_i were then used to define fitting and interpolation errors within exponential plus linear regressions.

For D_r values, systematic errors accommodate uncertainty in radionuclide conversion factors (5%), β attenuation coefficients (5%), matrix density (0.20 $g.cm^{-3}$), vertical thickness of sampled section (specific to sample collection device), saturation moisture content (3%), moisture content attenuation (2%) and burial moisture content (25% relative, unless direct evidence exists of the magnitude and period of differing content). Experimental errors are associated with radionuclide quantification for each sample by Ge gamma spectrometry.

The propagation of these errors through to age calculation was quantified using the expression,

$$\sigma y\ (\delta y/\delta x) = (\Sigma\ ((\delta y/\delta x_n).\sigma x_n)^2)^{1/2} \qquad \textbf{Eq. 2}$$

where y is a value equivalent to that function comprising terms x_n and where σy and σx_n are associated uncertainties.

Errors on age estimates are presented as combined systematic and experimental errors and experimental errors alone. The former (combined) error should be considered when comparing luminescence ages herein with independent chronometric controls. The latter assumes systematic errors are common to luminescence age estimates generated by means identical to those detailed herein and enable direct comparison with those estimates.

Fig. 1 Signal Calibration

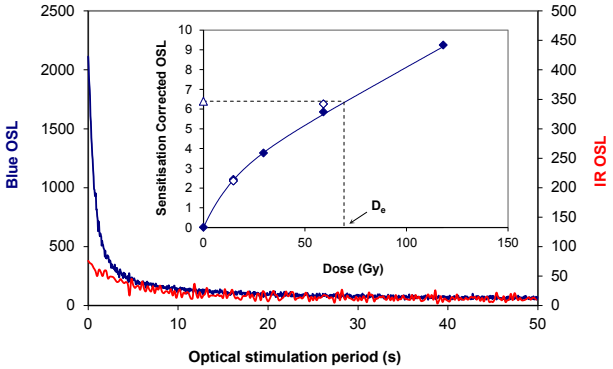

Fig. 2 Dose Recovery

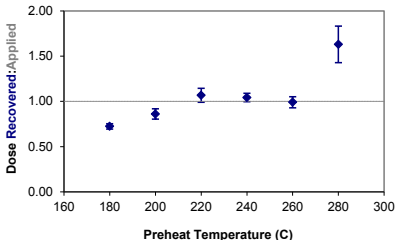

Fig. 3 Inter-aliquot D_e distribution

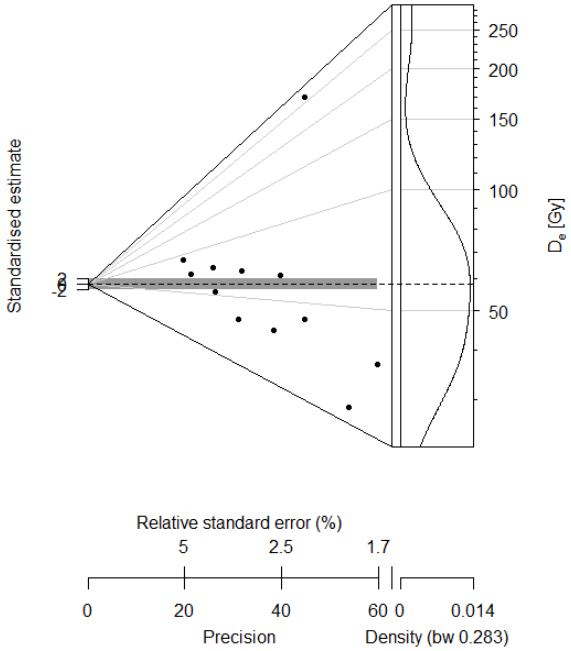

Fig. 4 Signal Analysis

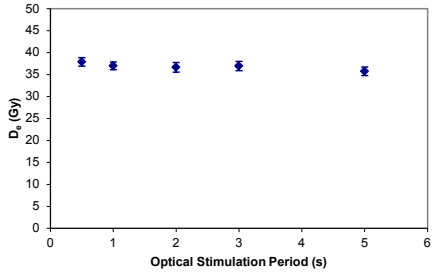

Fig. 5 U Decay Activity

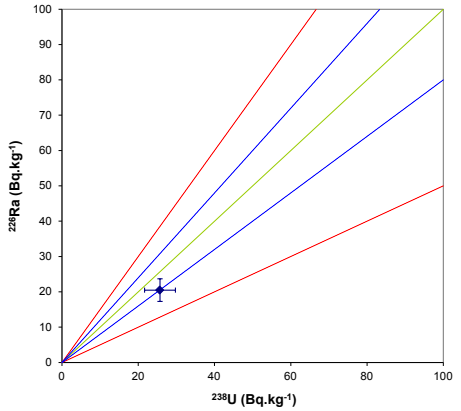

Fig. 6 Age Range

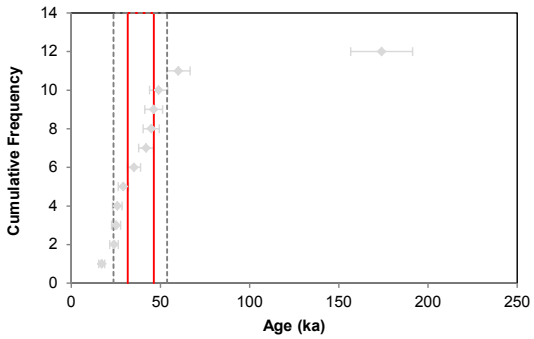

Fig. 1 Signal Calibration Natural blue and laboratory-induced infrared (IR) OSL signals. Detectable IR signal decays are diagnostic of feldspar contamination. Inset, the natural blue OSL signal (open triangle) of each aliquot is calibrated against known laboratory doses to yield equivalent dose (D_e) values. Repeats of low and high doses (open diamonds) illustrate the success of sensitivity correction.

Fig. 2 Dose Recovery The acquisition of D_e values is necessarily predicated upon thermal treatment of aliquots succeeding environmental and laboratory irradiation. The Dose Recovery test quantifies the combined effects of thermal transfer and sensitisation on the natural signal using a precise lab dose to simulate natural dose. Based on this an appropriate thermal treatment is selected to generate the final D_e value.

Fig. 3 Inter-aliquot D_e distribution Abanico plot of inter-aliquot statistical concordance in D_e values derived from **natural** irradiation. Discordant data (those points lying beyond **±2 standardised ln D_e**) reflect heterogeneous dose absorption and/or inaccuracies in calibration.

Fig. 4 Signal Analysis Statistically significant increase in **natural** D_e value with signal stimulation period is indicative of a partially-bleached signal, provided a significant increase in D_e results from **simulated partial bleaching** followed by insignificant adjustment in D_e for simulated **zero** and **full bleach** conditions. Ages from such samples are considered maximum estimates. In the absence of a significant rise in D_e with stimulation time, simulated partial bleaching and zero/full bleach tests are not assessed.

Fig. 5 U Activity Statistical concordance (equilibrium) in the activities of the daughter radioisotope ^{226}Ra with its parent ^{238}U may signify the temporal stability of D_r emissions from these chains. Significant differences (disequilibrium; >50%) in activity indicate addition or removal of isotopes creating a time-dependent shift in D_r values and increased uncertainty in the accuracy of age estimates. A 20% disequilibrium marker is also shown.

Fig. 6 Age Range The Cumulative frequency plot indicates the inter-aliquot variability in age. It also shows the **mean age range**; an estimate of sediment burial period based on mean D_e and D_r values with associated analytical uncertainties. The **maximum influence** of temporal variations in D_r forced by minima-maxima variation in moisture content and overburden thickness is outlined and may prove instructive where there is uncertainty in these parameters. However the combined extremes represented should not be construed as preferred age estimates.

Sample: GL17150 Quartz

Fig. 1 Signal Calibration

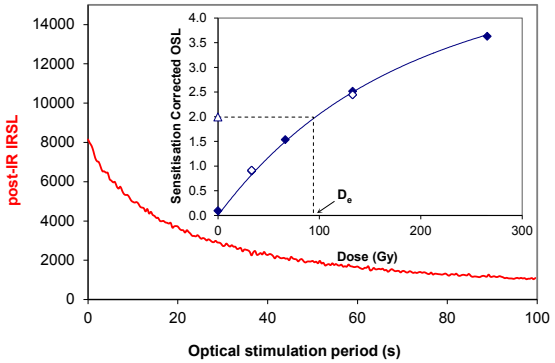

Fig. 1 Signal Calibration Natural post-IR IRSL signal stimulated at 250°C. Inset, the natural post-IR IRSL signal (open triangle) of each aliquot is calibrated against known laboratory doses to yield equivalent dose (D_e) values. Repeats of low and high doses (open diamonds) illustrate the success of sensitivity correction.

Fig. 2 Dose Recovery

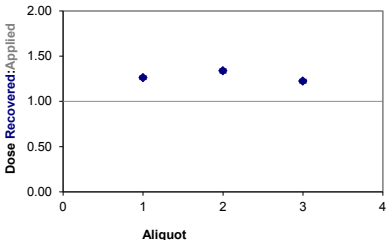

Fig. 2 Dose Recovery The acquisition of D_e values is necessarily predicated upon thermal treatment of aliquots succeeding environmental and laboratory irradiation. The Dose Recovery test quantifies the combined effects of thermal transfer and sensitisation on the natural signal using a precise lab dose to simulate natural dose. Based on this the likely accuracy of D_e produced by a SAR protocol that uses a 300°C, 60s preheat can be assessed.

Fig. 3 Inter-aliquot D_e distribution

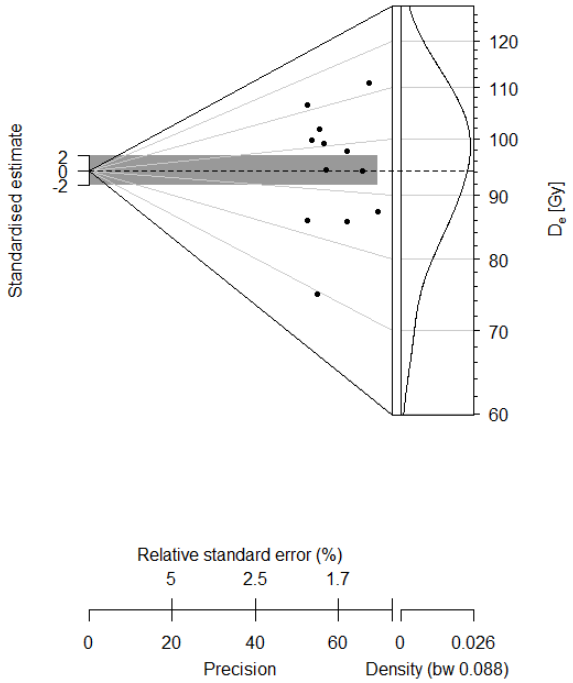

Fig. 3 Inter-aliquot D_e distribution Abanico plot of inter-aliquot statistical concordance in D_e values derived from **natural** irradiation. Discordant data (those points lying beyond ±2 standardised ln D_e) reflect heterogeneous dose absorption and/or inaccuracies in calibration.

Fig. 4 Signal Analysis

Applies only to OSL dating of quartz

Fig. 4 Signal Analysis applies only to OSL dating of quartz.

Fig. 5 U Decay Activity

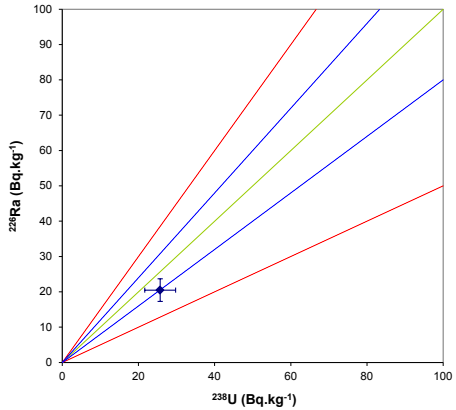

Fig. 5 U Activity Statistical concordance (equilibrium) in the activities of the daughter radioisotope ^{226}Ra with its parent ^{238}U may signify the temporal stability of D_r emissions from these chains. Significant differences (disequilibrium; >50%) in activity indicate addition or removal of isotopes creating a time-dependent shift in D_r values and increased uncertainty in the accuracy of age estimates. A 20% disequilibrium marker is also shown.

Fig. 6 Age Range

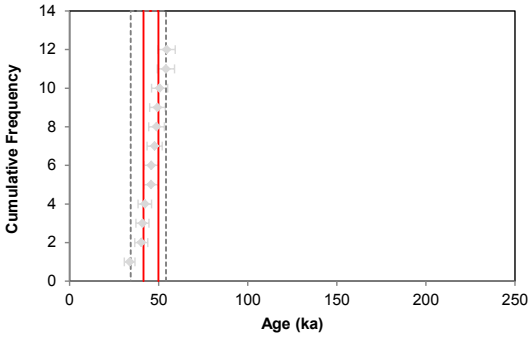

Fig. 6 Age Range The Cumulative frequency plot indicates the inter-aliquot variability in age. It also shows the **mean age range**; an estimate of sediment burial period based on mean D_e and D_r values with associated analytical uncertainties. The **maximum influence** of temporal variations in D_r forced by minima-maxima variation in moisture content and overburden thickness is outlined and may prove instructive where there is uncertainty in these parameters. However the combined extremes represented should not be construed as preferred age estimates.

Sample: GL17150 K-feldspar

References

Adamiec, G. and Aitken, M.J. (1998) Dose-rate conversion factors: new data. *Ancient TL*, 16, 37-50.

Agersnap-Larsen, N., Bulur, E., Bøtter-Jensen, L. and McKeever, S.W.S. (2000) Use of the LM-OSL technique for the detection of partial bleaching in quartz. *Radiation Measurements*, 32, 419-425.

Aitken, M. J. (1998) An introduction to optical dating: the dating of Quaternary sediments by the use of photon-stimulated luminescence. Oxford University Press.

Bailey, R.M., Singarayer, J.S. , Ward, S. and Stokes, S. (2003) Identification of partial resetting using D_e as a function of illumination time. *Radiation Measurements*, 37, 511-518.

Bateman, M.D., Frederick, C.D., Jaiswal, M.K., Singhvi, A.K. (2003) Investigations into the potential effects of pedoturbation on luminescence dating. *Quaternary Science Reviews*, 22, 1169-1176.

Bateman, M.D., Boulter, C.H., Carr, A.S., Frederick, C.D., Peter, D. and Wilder, M. (2007) Detecting post-depositional sediment disturbance in sandy deposits using optical luminescence. *Quaternary Geochronology*, 2, 57-64.

Berger, G.W. (2003). Luminescence chronology of late Pleistocene loess-paleosol and tephra sequences near Fairbanks, Alaska. *Quaternary Research*, 60, 70-83.

Bøtter-Jensen, L., Mejdahl, V. and Murray, A.S. (1999) New light on OSL. *Quaternary Science Reviews*, 18, 303-310.

Bøtter-Jensen, L., McKeever, S.W.S. and Wintle, A.G. (2003) Optically Stimulated Luminescence Dosimetry. Elsevier, Amsterdam.

Dietze, M., Kreutzer, S., Burow, C., Fuchs, M.C., Fischer, M., Schmidt, C. (2016) The abanico plot: visualising chronometric data with individual standard errors. *Quaternary Geochronology*, 31, 1-7.

Duller, G.A.T (2003) Distinguishing quartz and feldspar in single grain luminescence measurements. *Radiation Measurements*, 37, 161-165.

Galbraith, R. F., Roberts, R. G., Laslett, G. M., Yoshida, H. and Olley, J. M. (1999) Optical dating of single and multiple grains of quartz from Jinmium rock shelter (northern Australia): Part I, Experimental design and statistical models. *Archaeometry*, 41, 339-364.

Gliganic, L.A., May, J.-H. and Cohen, T.J. (2015). All mixed up: using single-grain equivalent dose distributions to identify phases of pedogenic mixing on a dryland alluvial fan. *Quaternary International*, 362, 23-33.

Gliganic, L.A., Cohen, T.J., Slack, M. and Feathers, J.K. (2016) Sediment mixing in Aeolian sandsheets identified and quantified using single-grain optically stimulated luminescence. *Quaternary Geochronology*, 32, 53-66.

Huntley, D.J., Godfrey-Smith, D.I. and Thewalt, M.L.W. (1985) Optical dating of sediments. *Nature*, 313, 105-107.

Hubbell, J.H. (1982) Photon mass attenuation and energy-absorption coefficients from 1keV to 20MeV. *International Journal of Applied Radioisotopes*, 33, 1269-1290.

Jacobs, A., Wintle, A.G., Duller, G.A.T, Roberts, R.G. and Wadley, L. (2008) New ages for the post-Howiesons Poort, late and finale middle stone age at Sibdu, South Africa. *Journal of Archaeological Science*, 35, 1790-1807.

Li, B., Roberts, R.G., Jacobs, Z. and Li, S-H (2014) A single-aliquot luminescence dating procedure for K-feldpsar based on the dose-dependent MET-pIRIR signal sensitivity. Quaternary Geochronology, 20, 51-64.

Lombard, M., Wadley, L., Jacobs, Z., Mohapi, M. and Roberts, R.G. (2011) Still Bay and serrated points from the Umhlatuzana rock shelter, Kwazulu-Natal, South Africa. *Journal of Archaeological Science*, 37, 1773-1784.

Markey, B.G., Bøtter-Jensen, L., and Duller, G.A.T. (1997) A new flexible system for measuring thermally and optically stimulated luminescence. *Radiation Measurements*, 27, 83-89.

Mejdahl, V. (1979) Thermoluminescence dating: beta-dose attenuation in quartz grains. *Archaeometry*, 21, 61-72.

Murray, A.S. and Olley, J.M. (2002) Precision and accuracy in the Optically Stimulated Luminescence dating of sedimentary quartz: a status review. *Geochronometria*, 21, 1-16.

Murray, A.S. and Wintle, A.G. (2000) Luminescence dating of quartz using an improved single-aliquot regenerative-dose protocol. *Radiation Measurements*, 32, 57-73.

Murray, A.S. and Wintle, A.G. (2003) The single aliquot regenerative dose protocol: potential for improvements in reliability. *Radiation Measurements*, 37, 377-381.

Murray, A.S., Olley, J.M. and Caitcheon, G.G. (1995) Measurement of equivalent doses in quartz from contemporary water-lain sediments using optically stimulated luminescence. *Quaternary Science Reviews*, 14, 365-371.

Olley, J.M., Murray, A.S. and Roberts, R.G. (1996) The effects of disequilibria in the Uranium and Thorium decay chains on burial dose rates in fluvial sediments. *Quaternary Science Reviews*, 15, 751-760.

Olley, J.M., Caitcheon, G.G. and Murray, A.S. (1998) The distribution of apparent dose as determined by optically stimulated luminescence in small aliquots of fluvial quartz: implications for dating young sediments. *Quaternary Science Reviews*, 17, 1033-1040.

Olley, J.M., Caitcheon, G.G. and Roberts R.G. (1999) The origin of dose distributions in fluvial sediments, and the prospect of dating single grains from fluvial deposits using -optically stimulated luminescence. *Radiation Measurements,* 30**,** 207-217.

Olley, J.M., Pietsch, T. and Roberts, R.G. (2004) Optical dating of Holocene sediments from a variety of geomorphic settings using single grains of quartz. *Geomorphology*, 60, 337-358.

Pawley, S.M., Toms, P.S., Armitage, S.J., Rose, J. (2010) Quartz luminescence dating of Anglian Stage fluvial sediments: Comparison of SAR age estimates to the terrace chronology of the Middle Thames valley, UK. *Quaternary Geochronology*, 5, 569-582.

Prescott, J.R. and Hutton, J.T. (1994) Cosmic ray contributions to dose rates for luminescence and ESR dating: large depths and long-term time variations. *Radiation Measurements*, 23, 497-500.

Singhvi, A.K., Bluszcz, A.., Bateman, M.D., Someshwar Rao, M. (2001). Luminescence dating of loess-palaeosol sequences and coversands: methodological aspects and palaeoclimatic implications. *Earth Science Reviews*, 54, 193-211.

Smith, B.W., Rhodes, E.J., Stokes, S., Spooner, N.A. (1990) The optical dating of sediments using quartz. *Radiation Protection Dosimetry*, 34, 75-78.

Spooner, N.A. (1993) The validity of optical dating based on feldspar. Unpublished D.Phil. thesis, Oxford University.

Templer, R.H. (1985) The removal of anomalous fading in zircons. *Nuclear Tracks and Radiation Measurements*, 10, 531-537.

Thomsen, K.J., Murray, A.S., Jain, M. and Botter-Jensen, L. (2008) Laboratory fading rates of various luminescence signals from feldspar-rich sediment extracts. *Radiation Measurements*, 43, 1474-1486.

Wallinga, J. (2002) Optically stimulated luminescence dating of fluvial deposits: a review. *Boreas* 31, 303-322.

Wintle, A.G. (1973) Anomalous fading of thermoluminescence in mineral samples. *Nature*, 245, 143-144.

Zimmerman, D. W. (1971) Thermoluminescent dating using fine grains from pottery. *Archaeometry*, 13, 29-52.

University of Gloucestershire

Luminescence dating laboratory

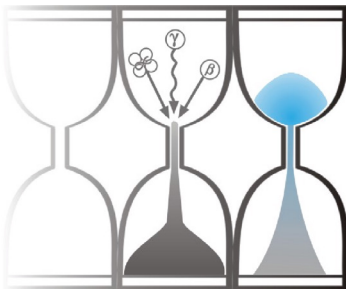

Paired Quartz & K-Feldspar Optical dating of sediments:
Triton Knoll Borehole (26.05-26.90 m), UK

to

Dr C. Mellett
Wessex Archaeology

Analysis & Reporting, Prof. P.S. Toms
Sample Preparation & Measurement, Mr J.C. Wood
14 January 2019

Contents

Scope of Report

This is a standard report of the Luminescence dating laboratory, University of Gloucestershire. In large part, the document summarises the processes, diagnostics and data drawn upon to deliver Table 1. A conclusion on the analytical validity of each sample's optical age estimate is expressed in Table 2; where there are caveats, the reader is directed to the relevant section of the report that explains the issue further in general terms.

Copyright Notice

Field Code	Lab Code	Overburden (m)	Grain size (μm)	Moisture content (%)	NaI γ-spectrometry (*in situ*) γ D_r ($Gy.ka^{-1}$)	Ge γ-spectrometry (*ex situ*)			Internal β D_r ($Gy.ka^{-1}$)	External β D_r ($Gy.ka^{-1}$)	External γ D_r ($Gy.ka^{-1}$)	Cosmic D_r ($Gy.ka^{-1}$)	Preheat (°C for 10s)	Low Dose Repeat Ratio	High Dose Repeat Ratio	Post-IR OSL Ratio
						K (%)	Th (ppm)	U (ppm)								
BHA03a – 26.05-26.90 m	GL18025 Quartz	26.22	125-180	16 ± 4	-	1.43 ± 0.10	6.70 ± 0.48	1.44 ± 0.13	-	1.12 ± 0.13	0.68 ± 0.10	0.01 ± 0.00	260	1.04 ± 0.03	1.03 ± 0.08	0.98 ± 0.03
	GL18025 K-Feldspar								0.57 ± 0.11				-	1.00 ± 0.01	0.99 ± 0.01	-

Field Code	Lab Code	Total D_r ($Gy.ka^{-1}$)	D_e (Gy)	Age (ka)
BHA03a – 26.05-26.90 m	GL18025 Quartz	1.82 ± 0.16	276.9 ± 26.9	152.2 ± 20.0 (18.5)
	GL18025 K-Feldspar	2.38 ± 0.19	862.5 ± 47.8	361.8 ± 35.6 (31.7)

Table 1 D_r, D_e and Age data of submitted samples located at c. 53°N, 1°E, 0m. Age estimates expressed relative to year of sampling. Uncertainties in age are quoted at 1σ confidence, are based on analytical errors and reflect combined systematic and experimental variability and (in parenthesis) experimental variability alone (see 6.0). **Blue** indicates samples with accepted age estimates, **red**, age estimates with caveats (see Table 2).

Generic considerations	Field Code	Lab Code	Sample specific considerations
Absence of *in situ* γ spectrometry data (see section 4.0)	BHA03a – 26.05-26.90 m	GL18025 Quartz	Significant feldspar contamination (see section 3.1.1, Table 1 and Fig. 1) Accept as minimum age estimate
		GL18025 K-Feldspar	Failed Dose Recovery test (see section 3.1.2 and Fig. 2) Accept as maximum age estimate

Table 2 Analytical validity of sample suite age estimates and caveats for consideration

1.0 Mechanisms and principles

Upon exposure to ionising radiation, electrons within the crystal lattice of insulating minerals are displaced from their atomic orbits. Whilst this dislocation is momentary for most electrons, a portion of charge is redistributed to meta-stable sites (traps) within the crystal lattice. In the absence of significant optical and thermal stimuli, this charge can be stored for extensive periods. The quantity of charge relocation and storage relates to the magnitude and period of irradiation. When the lattice is optically or thermally stimulated, charge is evicted from traps and may return to a vacant orbit position (hole). Upon recombination with a hole, an electron's energy can be dissipated in the form of light generating crystal luminescence providing a measure of dose absorption.

In this report, both quartz and K-feldspar were segregated for dating. The utility of quartz as a minerogenic dosimeter lies in the stability of its datable signal over the mid to late Quaternary period, predicted through isothermal decay studies (e.g. Smith *et al*., 1990; retention lifetime 630 Ma at 20°C) and evidenced by optical age estimates concordant with independent chronological controls (e.g. Murray and Olley, 2002). This stability is in contrast to the anomalous fading of comparable signals commonly observed for other ubiquitous sedimentary minerals such as feldspar and zircon (Wintle, 1973; Templer, 1985; Spooner, 1993). However, recent studies of K-feldspar have identified a non-fading signal (Thomsen et al., 2008). And with the ability of feldspar to accumulate signal over periods longer than that of quartz, paired quartz and K-feldspar dating is a pragmatic approach for samples that may date earlier than the Late Pleistocene.

Optical age estimates of sedimentation (Huntley *et al*., 1985) are premised upon reduction of the minerogenic time dependent signal (Optically Stimulated Luminescence, OSL) to zero through exposure to sunlight and, once buried, signal reformulation by absorption of litho- and cosmogenic radiation. The signal accumulated post burial acts as a dosimeter recording total dose absorption, converting to a chronometer by estimating the rate of dose absorption quantified through the assay of radioactivity in the surrounding lithology and streaming from the cosmos.

$$\text{Age} = \frac{\text{Mean Equivalent Dose } (D_e, \text{ Gy})}{\text{Mean Dose Rate } (D_r, \text{ Gy.ka}^{-1})}$$

Aitken (1998) and Bøtter-Jensen *et al*. (2003) offer a detailed review of optical dating.

2.0 Sample Preparation

One sediment core was collected within opaque tubing and submitted for Optical dating. To preclude optical erosion of the datable signal prior to measurement, the sample was opened and prepared under controlled laboratory illumination provided by Encapsulite RB-10 (red) filters. To isolate that material potentially exposed to daylight during sampling, sediment located within 10 mm of each core face was removed.

The remaining sample was dried and then sieved. The fine sand fraction was segregated and subjected to acid and alkaline digestion (10% HCl, 15% H_2O_2) to attain removal of carbonate and organic components respectively. The sample was then divided in two. For one half, a further acid digestion in HF (40%, 60 mins) was used to etch the outer 10-15 μm layer affected by α radiation and degrade each samples' feldspar content. During HF treatment, continuous magnetic stirring was used to effect isotropic etching of grains. 10% HCl was then added to remove acid soluble fluorides. Each sample was dried, resieved and quartz isolated from the remaining heavy mineral fraction using a sodium polytungstate density separation at 2.68g.cm^{-3}. For the second half, density separations at 2.53 and 2.58 g cm^{-3} were undertaken to isolate the K-feldspar fraction. Twelve 8 mm multi-grain aliquots (*c*. 3-6 mg) of quartz and K-feldspar were then mounted on aluminium discs for determination of D_e values.

All drying was conducted at 40°C to prevent thermal erosion of the signal. All acids and alkalis were Analar grade. All dilutions (removing toxic-corrosive and non-minerogenic luminescence-bearing substances) were conducted with distilled water to prevent signal contamination by extraneous particles.

3.0 Acquisition and accuracy of D_e value

All minerals naturally exhibit marked inter-sample variability in luminescence per unit dose (sensitivity). Therefore, the estimation of D_e acquired since burial requires calibration of the natural signal using known amounts of laboratory dose. D_e values were quantified using a single-aliquot regenerative-dose (SAR) protocol (Murray and Wintle 2000, 2003 for quartz; Li et al., 2014 for K-feldspar) facilitated by a Risø TL-DA-15 irradiation-stimulation-detection system (Markey *et al*., 1997; Bøtter-Jensen *et al*., 1999). Within this apparatus, optical signal stimulation of quartz is provided by an assembly of blue diodes (5 packs of 6 Nichia NSPB500S), filtered to 470±80 nm conveying 15 $mW.cm^{-2}$ using a 3 mm Schott GG420 positioned in front of each diode pack. Infrared (IR) stimulation for K-feldspars is provided by 6 IR diodes (Telefunken TSHA 6203) stimulating at 875±80nm delivering ~5 $mW.cm^{-2}$. Stimulated photon emissions from quartz aliquots are in the ultraviolet (UV) range and were filtered from stimulating photons by 7.5 mm HOYA U-340 glass and detected by an EMI 9235QA photomultiplier fitted with a blue-green sensitive bialkali photocathode. K-feldpar emissions were filtered by 2 mm Schott BG-39 and 3mm Schott BG-3 glass. Aliquot irradiation was conducted using a 1.48 GBq $^{90}Sr/^{90}Y$ β source calibrated for multi-grain aliquots of 125-180 μm quartz and feldspar against the 'Hotspot 800' ^{60}Co γ source located at the National Physical Laboratory (NPL), UK.

SAR by definition evaluates D_e through measuring the natural signal (Fig. 1) of a single aliquot and then regenerating that aliquot's signal by using known laboratory doses to enable calibration. For each aliquot, five different regenerative-doses were administered so as to image dose response. D_e values for each aliquot were then interpolated, and associated counting and fitting errors calculated, by way of exponential plus linear regression (Fig. 1). Weighted (geometric) mean D_e values were calculated from 12 aliquots using the central age model outlined by Galbraith *et al*. (1999) and are quoted at 1σ confidence (Table 1). The accuracy with which D_e equates to total absorbed dose and that dose absorbed since burial was assessed. The former can be considered a function of laboratory factors, the latter, one of environmental issues. Diagnostics were deployed to estimate the influence of these factors and criteria instituted to optimise the accuracy of D_e values.

3.1 Laboratory Factors

3.1.1 Feldspar contamination of quartz

The propensity of feldspar signals to fade and underestimate age, coupled with their higher sensitivity relative to quartz makes it imperative to quantify feldspar contamination. At room temperature, feldspars generate a signal (IRSL; Fig. 1) upon exposure to IR whereas quartz does not. The signal from feldspars contributing to OSL can be depleted by prior exposure to IR. For all aliquots the contribution of any remaining feldspars was estimated from the OSL IR depletion ratio (Duller, 2003). The influence of IR depletion on the OSL signal can be illustrated by comparing the regenerated post-IR OSL D_e with the applied regenerative-dose. If the addition to OSL by feldspars is insignificant, then the repeat dose ratio of OSL to post-IR OSL should be statistically consistent with unity (Table 1). If any aliquots do not fulfil this criterion, then the sample age estimate should be accepted tentatively. The source of feldspar contamination is rarely rooted in sample preparation; it predominantly results from the occurrence of feldspars as inclusions within quartz.

3.1.2 Preheating

Preheating aliquots between irradiation and optical stimulation is necessary to ensure comparability between natural and laboratory-induced signals. However, the multiple irradiation and preheating steps that are required to define single-aliquot regenerative-dose response leads to signal sensitisation, rendering calibration of the natural signal inaccurate.

The SAR protocol (Murray and Wintle, 2000; 2003) enables this sensitisation to be monitored and corrected using a test dose to track signal sensitivity between irradiation-preheat steps. In the case of quartz a 5 Gy test dose preheated to 220°C for 10s was used. For K-feldspar a 30 Gy test dose and 300°C preheat for 60s was applied (Li et al. 2014), However, the accuracy of sensitisation correction for both natural and laboratory signals can be preheat dependent.

The Dose Recovery test was used to assess the optimal preheat temperature for accurate correction and calibration of the time dependent signal. Dose Recovery (Fig. 2) attempts to quantify the combined effects of thermal transfer and sensitisation on the natural signal, using a precise lab dose to simulate natural dose. The ratio between the applied dose and recovered D_e value should be statistically concordant with unity. For this diagnostic, in the case of quartz, 6 aliquots were each assigned a 10 s preheat between 180°C and 280°C. For the K-feldspar fraction, the efficacy of the 300°C, 60s preheat in Dose Recovery was assessed from the average of three aliquots.

That preheat treatment fulfilling the criterion of accuracy within the Dose Recovery test was selected to generate the final D_e value from a further 12 aliquots. Further thermal treatments, prescribed by Murray and Wintle (2000; 2003), were applied to optimise accuracy and precision. Optical stimulation of quartz occurred at 125ºC in order to minimise effects associated with photo-transferred thermoluminescence and maximise signal to noise ratios (Murray and Wintle, 2000; 2003). For K-feldspar, optical stimulation was performed at 50°C then 200°C to remove the fading signal, with the non-fading signal then measured at 250°C (Li et al., 2014). Inter-cycle optical stimulation was conducted at 280ºC for quartz and 320ºC for K-feldspar to minimise recuperation.

3.1.3 Internal consistency

Abanico plots (Dietze *et al*., 2016) are used to illustrate inter-aliquot D_e variability (Fig. 3). D_e values are standardised relative to the central D_e value for natural signals and are described as overdispersed when >5% lie beyond $\pm 2\sigma$ of the standardising value; resulting from a heterogeneous absorption of burial dose and/or response to the SAR protocol. For multi-grain aliquots, overdispersion of natural signals does not necessarily imply inaccuracy. However where overdispersion is observed for regenerated signals, the efficacy of sensitivity correction may be problematic. Murray and Wintle (2000; 2003) suggest repeat dose ratios (Table 1) offer a measure of SAR protocol success, whereby ratios ranging across 0.9-1.1 represent effective sensitivity correction. However, this variation of repeat dose ratios in the high-dose region can have a significant impact on D_e interpolation.

3.2 Environmental factors

3.2.1 Incomplete zeroing

Post-burial OSL signals residual of pre-burial dose absorption can result where pre-burial sunlight exposure is limited in spectrum, intensity and/or period, leading to age overestimation. This effect is particularly acute for material eroded and redeposited sub-aqueously (Olley *et al*., 1998, 1999; Wallinga, 2002) and exposed to a burial dose of <20 Gy (e.g. Olley *et al*., 2004), has some influence in sub-aerial contexts but is rarely of consequence where aerial transport has occurred. Within single-aliquot regenerative-dose optical dating there are two diagnostics of partial resetting (or bleaching); signal analysis (Agersnap-Larsen *et al*., 2000; Bailey *et al*., 2003) and inter-aliquot D_e distribution studies (Murray *et al*., 1995).

Within this stud signal analysis, which is only applicable to quartz, was used to quantify the change in D_e value with respect to optical stimulation time for multi-grain aliquots. This exploits the existence of traps within minerogenic dosimeters that bleach with different efficiency for a given wavelength of light to verify partial bleaching. D_e (t) plots (Fig. 4; Bailey *et al*., 2003) are constructed from separate integrals of signal decay as laboratory optical stimulation progresses. A statistically significant increase in natural D_e (t) is indicative of partial bleaching assuming three conditions are fulfilled. Firstly, that a statistically significant increase in D_e (t) is observed when partial bleaching is simulated within the laboratory. Secondly, that there is no significant rise in D_e (t) when full bleaching is simulated. Finally, there should be

no significant augmentation in D_e (t) when zero dose is simulated. Where partial bleaching is detected, the age derived from the sample should be considered a maximum estimate only. However, the utility of signal analysis is strongly dependent upon a samples pre-burial experience of sunlight's spectrum and its residual to post-burial signal ratio. Given in the majority of cases, the spectral exposure history of a deposit is uncertain, the absence of an increase in natural D_e (t) does not necessarily testify to the absence of partial bleaching.

Where requested and feasible, the insensitivities of multi-grain single-aliquot signal analysis may be circumvented by inter-aliquot D_e distribution studies, which can be attempted on both quartz and K-feldspars. This analysis uses aliquots of single sand grains to quantify inter-grain D_e distribution. At present, it is contended that asymmetric inter-grain D_e distributions are symptomatic of partial bleaching and/or pedoturbation (Murray *et al*., 1995; Olley *et al*., 1999; Olley *et al*., 2004; Bateman *et al*., 2003). For partial bleaching at least, it is further contended that the D_e acquired during burial is located in the minimum region of such ranges. The mean and breadth of this minimum region is the subject of current debate, as it is additionally influenced by heterogeneity in microdosimetry, variable inter-grain response to SAR, residual to post-burial signal ratios and, in the case of K-feldspar, inter-grain variations in K content.

3.2.2 Turbation

As noted in section 3.1.1, the accuracy of sedimentation ages can further be controlled by post-burial trans-strata grain movements forced by pedo- or cryoturbation. Berger (2003) contends pedogenesis prompts a reduction in the apparent sedimentation age of parent material through bioturbation and illuviation of younger material from above and/or by biological recycling and resetting of the datable signal of surface material. Berger (2003) proposes that the chronological products of this remobilisation are A-horizon age estimates reflecting the cessation of pedogenic activity, Bc/C-horizon ages delimiting the maximum age for the initiation of pedogenesis with estimates obtained from Bt-horizons providing an intermediate age 'close to the age of cessation of soil development'. Singhvi et al. (2001), in contrast, suggest that B and C-horizons closely approximate the age of the parent material, the A-horizon, that of the 'soil forming episode'. Recent analyses of inter-aliquot D_e distributions have reinforced this complexity of interpreting burial age from pedoturbated deposits (Lombard *et al*., 2011; Gliganic *et al*., 2015; Jacobs *et al*., 2008; Bateman *et al*., 2007; Gliganic *et al*., 2016). At present there is no definitive post-sampling mechanism for the direct detection of and correction for post-burial sediment remobilisation. However, intervals of palaeosol evolution can be delimited by a maximum age derived from parent material and a minimum age obtained from a unit overlying the palaeosol. Inaccuracy forced by cryoturbation may be bidirectional, heaving older material upwards or drawing younger material downwards into the level to be dated. Cryogenic deformation of matrix-supported material is, typically, visible; sampling of such cryogenically-disturbed sediments can be avoided.

4.0 Acquisition and accuracy of D_r value

For lithogenic radiation external to the grains of quartz and K-feldspar, D_r values were defined through measurement of U, Th and K radionuclide concentration and conversion of these quantities into β and γ D_r values (Table 1). β contributions were estimated from sub-samples by laboratory-based γ spectrometry using an Ortec GEM-S high purity Ge coaxial detector system, calibrated using certified reference materials supplied by CANMET. γ dose rates can be estimated from *in situ* NaI gamma spectrometry or, where direct measurements are unavailable as in the present case, from laboratory-based Ge γ spectrometry. *In situ* measurements reduce uncertainty relating to potential heterogeneity in the γ dose field surrounding each sample. The level of U disequilibrium was estimated by laboratory-based Ge γ spectrometry. Estimates of radionuclide concentration were converted into D_r values (Adamiec and Aitken, 1998), accounting for D_r modulation forced by grain size (Mejdahl, 1979) and present moisture content (Zimmerman, 1971). Lithogenic radiation internal to K-feldspar grains was assumed to be derived from a K content of 12.5%. Cosmogenic D_r

values were calculated on the basis of sample depth, geographical position and matrix density (Prescott and Hutton, 1994).

The spatiotemporal validity of D_r values can be considered a function of five variables. Firstly, age estimates devoid of *in situ* γ spectrometry data should be accepted tentatively if the sampled unit is heterogeneous in texture or if the sample is located within 300 mm of strata consisting of differing texture and/or mineralogy. However, where samples are obtained throughout a vertical profile, consistent values of γ D_r based solely on laboratory measurements may evidence the homogeneity of the γ field and hence accuracy of γ D_r values. Secondly, disequilibrium can force temporal instability in U and Th emissions. The impact of this infrequent phenomenon (Olley *et al*., 1996) upon age estimates is usually insignificant given their associated margins of error. However, for samples where this effect is pronounced (>50% disequilibrium between ^{238}U and ^{226}Ra; Fig. 5), the resulting age estimates should be accepted tentatively. Thirdly, pedogenically-induced variations in matrix composition of B and C-horizons, such as radionuclide and/or mineral remobilisation, may alter the rate of energy emission and/or absorption. If D_r is invariant through a dated profile and samples encompass primary parent material, then element mobility is likely limited in effect. Fourthly, spatiotemporal detractions from present moisture content are difficult to assess directly, requiring knowledge of the magnitude and timing of differing contents. However, the maximum influence of moisture content variations can be delimited by recalculating D_r for minimum (zero) and maximum (saturation) content. Finally, temporal alteration in the thickness of overburden alters cosmic D_r values. Cosmic D_r often forms a negligible portion of total D_r. It is possible to quantify the maximum influence of overburden flux by recalculating D_r for minimum (zero) and maximum (surface sample) cosmic D_r.

5.0 Estimation of Age

Ages reported in Table 1 provide an estimate of sediment burial period based on mean D_e and D_r values and their associated analytical uncertainties. Uncertainty in age estimates is reported as a product of systematic and experimental errors, with the magnitude of experimental errors alone shown in parenthesis (Table 1). Cumulative frequency plots indicate the inter-aliquot variability in age (Fig. 6). The maximum influence of temporal variations in D_r forced by minima-maxima in moisture content and overburden thickness is also illustrated in Fig. 6. Where uncertainty in these parameters exists this age range may prove instructive, however the combined extremes represented should not be construed as preferred age estimates. The analytical validity of each sample is presented in Table 2.

6.0 Analytical uncertainty

All errors are based upon analytical uncertainty and quoted at 1σ confidence. Error calculations account for the propagation of systematic and/or experimental (random) errors associated with D_e and D_r values.

For D_e values, systematic errors are confined to laboratory β source calibration. Uncertainty in this respect is that combined from the delivery of the calibrating γ dose (1.2%; NPL, pers. comm.), the conversion of this dose for SiO_2 using the respective mass energy-absorption coefficient (2%; Hubbell, 1982) and experimental error, totalling 3.5%. Mass attenuation and bremsstrahlung losses during γ dose delivery are considered negligible. Experimental errors relate to D_e interpolation using sensitisation corrected dose responses. Natural and regenerated sensitisation corrected dose points (S_i) were quantified by,

$$S_i = (D_i - x.L_i) / (d_i - x.L_i) \qquad \textbf{Eq.1}$$

where D_i = Natural or regenerated OSL, initial 0.2 s

L_i = Background natural or regenerated OSL, final 5 s

d_i = Test dose OSL, initial 0.2 s

x = Scaling factor, 0.08

The error on each signal parameter is based on counting statistics, reflected by the square-root of measured values. The propagation of these errors within Eq. 1 generating σS_i follows the general formula given in Eq. 2. σS_i were then used to define fitting and interpolation errors within exponential plus linear regressions.

For D_r values, systematic errors accommodate uncertainty in radionuclide conversion factors (5%), β attenuation coefficients (5%), matrix density (0.20 $g.cm^{-3}$), vertical thickness of sampled section (specific to sample collection device), saturation moisture content (3%), moisture content attenuation (2%) and burial moisture content (25% relative, unless direct evidence exists of the magnitude and period of differing content). Experimental errors are associated with radionuclide quantification for each sample by Ge gamma spectrometry.

The propagation of these errors through to age calculation was quantified using the expression,

$$\sigma y\ (\delta y/\delta x) = (\Sigma\ ((\delta y/\delta x_n).\sigma x_n)^2)^{1/2} \qquad \textbf{Eq. 2}$$

where y is a value equivalent to that function comprising terms x_n and where σy and σx_n are associated uncertainties.

Errors on age estimates are presented as combined systematic and experimental errors and experimental errors alone. The former (combined) error should be considered when comparing luminescence ages herein with independent chronometric controls. The latter assumes systematic errors are common to luminescence age estimates generated by means identical to those detailed herein and enable direct comparison with those estimates.

Fig. 1 Signal Calibration

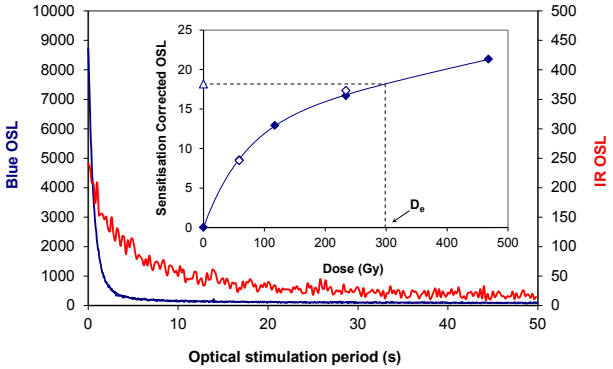

Fig. 1 Signal Calibration Natural blue and laboratory-induced infrared (IR) OSL signals. Detectable IR signal decays are diagnostic of feldspar contamination. Inset, the natural blue OSL signal (open triangle) of each aliquot is calibrated against known laboratory doses to yield equivalent dose (D_e) values. Repeats of low and high doses (open diamonds) illustrate the success of sensitivity correction.

Fig. 2 Dose Recovery The acquisition of D_e values is necessarily predicated upon thermal treatment of aliquots succeeding environmental and laboratory irradiation. The Dose Recovery test quantifies the combined effects of thermal transfer and sensitisation on the natural signal using a precise lab dose to simulate natural dose. Based on this an appropriate thermal treatment is selected to generate the final D_e value.

Fig. 3 Inter-aliquot D_e distribution Abanico plot of inter-aliquot statistical concordance in D_e values derived from **natural** irradiation. Discordant data (those points lying beyond **±2 standardised ln D_e**) reflect heterogeneous dose absorption and/or inaccuracies in calibration.

Fig. 4 Signal Analysis Statistically significant increase in **natural** D_e value with signal stimulation period is indicative of a partially-bleached signal, provided a significant increase in D_e results from **simulated partial bleaching** followed by insignificant adjustment in D_e for simulated **zero** and **full bleach** conditions. Ages from such samples are considered maximum estimates. In the absence of a significant rise in D_e with stimulation time, simulated partial bleaching and zero/full bleach tests are not assessed.

Fig. 5 U Activity Statistical concordance (equilibrium) in the activities of the daughter radioisotope ^{226}Ra with its parent ^{238}U may signify the temporal stability of D_r emissions from these chains. Significant differences (disequilibrium; >50%) in activity indicate addition or removal of isotopes creating a time-dependent shift in D_r values and increased uncertainty in the accuracy of age estimates. A 20% disequilibrium marker is also shown.

Fig. 6 Age Range The Cumulative frequency plot indicates the inter-aliquot variability in age. It also shows the **mean age range**; an estimate of sediment burial period based on mean D_e and D_r values with associated analytical uncertainties. The **maximum influence** of temporal variations in D_r forced by minima-maxima variation in moisture content and overburden thickness is outlined and may prove instructive where there is uncertainty in these parameters. However the combined extremes represented should not be construed as preferred age estimates.

Fig. 2 Dose Recovery

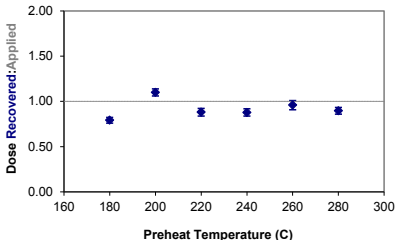

Fig. 3 Inter-aliquot D_e distribution

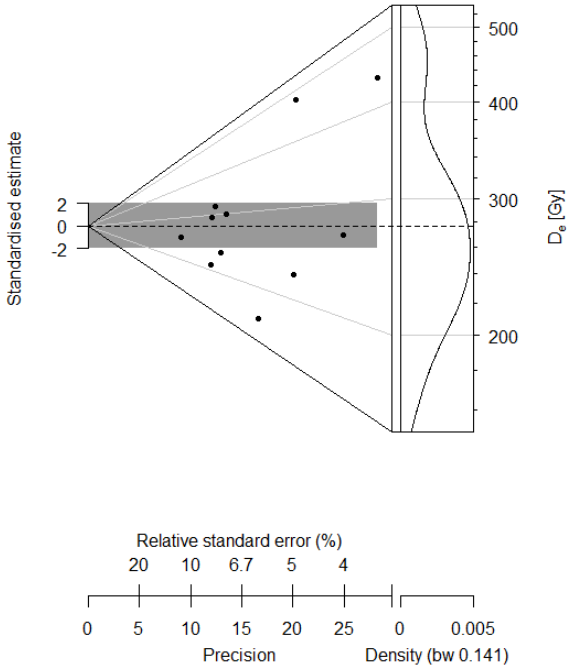

Fig. 4 Signal Analysis

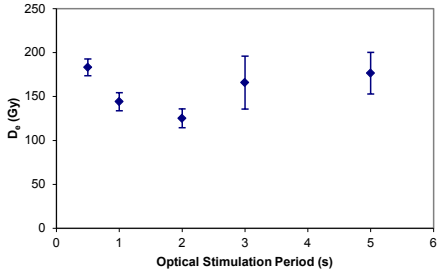

Fig. 5 U Decay Activity

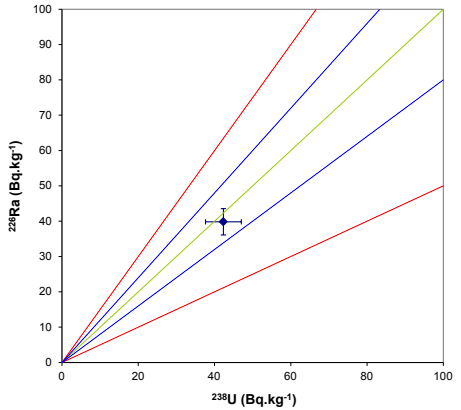

Fig. 6 Age Range

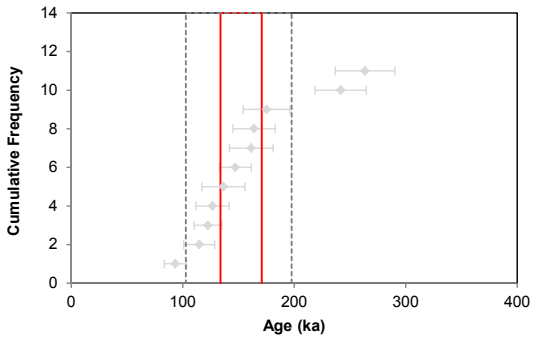

Sample: GL18025 Quartz

Fig. 1 Signal Calibration

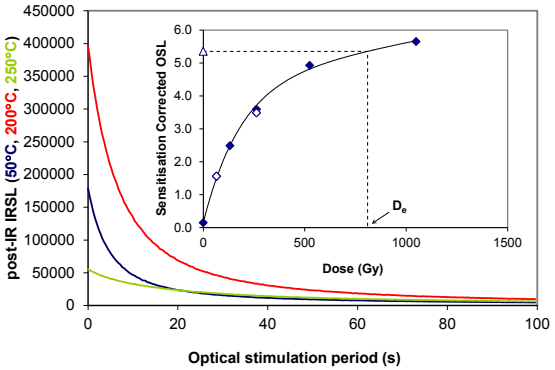

Fig. 2 Dose Recovery

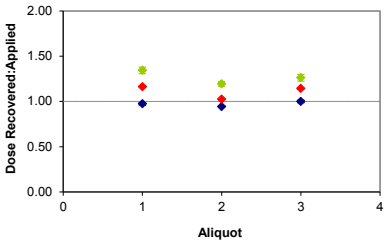

Fig. 3 Inter-aliquot D_e distribution

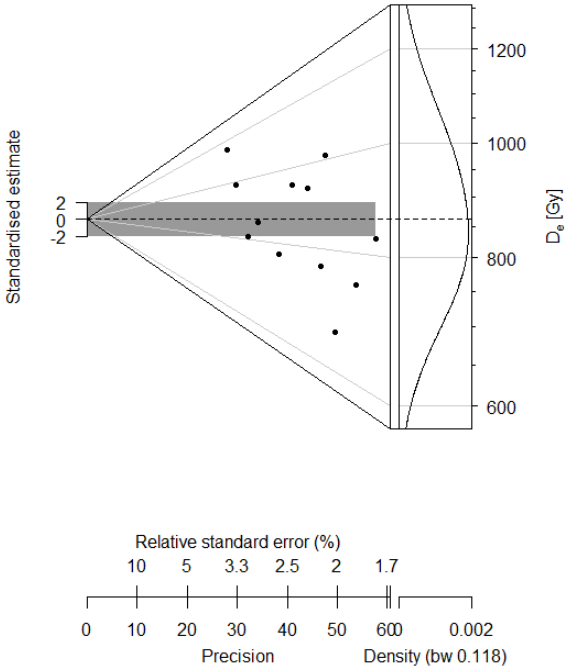

Fig. 4 Signal Analysis

Applies only to OSL dating of quartz

Fig. 5 U Decay Activity

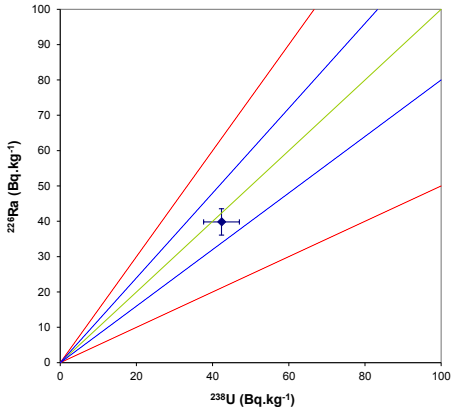

Fig. 6 Age Range

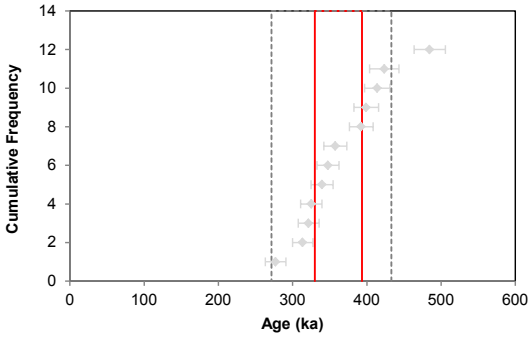

Fig. 1 Signal Calibration Natural post-IR IRSL signal stimulated at 50°C, 200°C and 250°C. The non-fading signal at 250°C is used to estimate the burial dose. Inset, the natural post-IR IRSL signal (open triangle) of each aliquot is calibrated against known laboratory doses to yield equivalent dose (D_e) values. Repeats of low and high doses (open diamonds) illustrate the success of sensitivity correction.

Fig. 2 Dose Recovery The acquisition of D_e values is necessarily predicated upon thermal treatment of aliquots succeeding environmental and laboratory irradiation. The Dose Recovery test quantifies the combined effects of thermal transfer and sensitisation on the natural signal using a precise lab dose to simulate natural dose. Based on this the likely accuracy of D_e produced by a SAR protocol that uses a 300°C, 60s preheat can be assessed. Outcomes for this test are shown for post-IR IRSL signals stimulated at 50°C, 200°C and 250°C.

Fig. 3 Inter-aliquot D_e distribution Abanico plot of inter-aliquot statistical concordance in D_e values derived from **natural** irradiation. Discordant data (those points lying beyond **±2 standardised ln D_e**) reflect heterogeneous dose absorption and/or inaccuracies in calibration.

Fig. 4 Signal Analysis applies only to OSL dating of quartz.

Fig. 5 U Activity Statistical concordance (equilibrium) in the activities of the daughter radioisotope ^{226}Ra with its parent ^{238}U may signify the temporal stability of D_r emissions from these chains. Significant differences (disequilibrium; >50%) in activity indicate addition or removal of isotopes creating a time-dependent shift in D_r values and increased uncertainty in the accuracy of age estimates. A 20% disequilibrium marker is also shown.

Fig. 6 Age Range The Cumulative frequency plot indicates the inter-aliquot variability in age. It also shows the **mean age range**; an estimate of sediment burial period based on mean D_e and D_r values with associated analytical uncertainties. The **maximum influence** of temporal variations in D_r forced by minima-maxima variation in moisture content and overburden thickness is outlined and may prove instructive where there is uncertainty in these parameters. However the combined extremes represented should not be construed as preferred age estimates.

Sample: GL18025 K-feldspar

References

Adamiec, G. and Aitken, M.J. (1998) Dose-rate conversion factors: new data. *Ancient TL*, 16, 37-50.

Agersnap-Larsen, N., Bulur, E., Bøtter-Jensen, L. and McKeever, S.W.S. (2000) Use of the LM-OSL technique for the detection of partial bleaching in quartz. *Radiation Measurements*, 32, 419-425.

Aitken, M. J. (1998) An introduction to optical dating: the dating of Quaternary sediments by the use of photon-stimulated luminescence. Oxford University Press.

Bailey, R.M., Singarayer, J.S. , Ward, S. and Stokes, S. (2003) Identification of partial resetting using D_e as a function of illumination time. *Radiation Measurements*, 37, 511-518.

Bateman, M.D., Frederick, C.D., Jaiswal, M.K., Singhvi, A.K. (2003) Investigations into the potential effects of pedoturbation on luminescence dating. *Quaternary Science Reviews*, 22, 1169-1176.

Bateman, M.D., Boulter, C.H., Carr, A.S., Frederick, C.D., Peter, D. and Wilder, M. (2007) Detecting post-depositional sediment disturbance in sandy deposits using optical luminescence. *Quaternary Geochronology*, 2, 57-64.

Berger, G.W. (2003). Luminescence chronology of late Pleistocene loess-paleosol and tephra sequences near Fairbanks, Alaska. *Quaternary Research*, 60, 70-83.

Bøtter-Jensen, L., Mejdahl, V. and Murray, A.S. (1999) New light on OSL. *Quaternary Science Reviews*, 18, 303-310.

Bøtter-Jensen, L., McKeever, S.W.S. and Wintle, A.G. (2003) Optically Stimulated Luminescence Dosimetry. Elsevier, Amsterdam.

Dietze, M., Kreutzer, S., Burow, C., Fuchs, M.C., Fischer, M., Schmidt, C. (2016) The abanico plot: visualising chronometric data with individual standard errors. *Quaternary Geochronology*, 31, 1-7.

Duller, G.A.T (2003) Distinguishing quartz and feldspar in single grain luminescence measurements. *Radiation Measurements*, 37, 161-165.

Galbraith, R. F., Roberts, R. G., Laslett, G. M., Yoshida, H. and Olley, J. M. (1999) Optical dating of single and multiple grains of quartz from Jinmium rock shelter (northern Australia): Part I, Experimental design and statistical models. *Archaeometry*, 41, 339-364.

Gliganic, L.A., May, J.-H. and Cohen, T.J. (2015). All mixed up: using single-grain equivalent dose distributions to identify phases of pedogenic mixing on a dryland alluvial fan. *Quaternary International*, 362, 23-33.

Gliganic, L.A., Cohen, T.J., Slack, M. and Feathers, J.K. (2016) Sediment mixing in Aeolian sandsheets identified and quantified using single-grain optically stimulated luminescence. *Quaternary Geochronology*, 32, 53-66.

Huntley, D.J., Godfrey-Smith, D.I. and Thewalt, M.L.W. (1985) Optical dating of sediments. *Nature*, 313, 105-107.

Hubbell, J.H. (1982) Photon mass attenuation and energy-absorption coefficients from 1keV to 20MeV. *International Journal of Applied Radioisotopes*, 33, 1269-1290.

Jacobs, A., Wintle, A.G., Duller, G.A.T, Roberts, R.G. and Wadley, L. (2008) New ages for the post-Howiesons Poort, late and finale middle stone age at Sibdu, South Africa. *Journal of Archaeological Science*, 35, 1790-1807.

Li, B., Roberts, R.G., Jacobs, Z. and Li, S-H (2014) A single-aliquot luminescence dating procedure for K-feldpsar based on the dose-dependent MET-pIRIR signal sensitivity. Quaternary Geochronology, 20, 51-64.

Lombard, M., Wadley, L., Jacobs, Z., Mohapi, M. and Roberts, R.G. (2011) Still Bay and serrated points from the Umhlatuzana rock shelter, Kwazulu-Natal, South Africa. *Journal of Archaeological Science*, 37, 1773-1784.

Markey, B.G., Bøtter-Jensen, L., and Duller, G.A.T. (1997) A new flexible system for measuring thermally and optically stimulated luminescence. *Radiation Measurements*, 27, 83-89.

Mejdahl, V. (1979) Thermoluminescence dating: beta-dose attenuation in quartz grains. *Archaeometry*, 21, 61-72.

Murray, A.S. and Olley, J.M. (2002) Precision and accuracy in the Optically Stimulated Luminescence dating of sedimentary quartz: a status review. *Geochronometria*, 21, 1-16.

Murray, A.S. and Wintle, A.G. (2000) Luminescence dating of quartz using an improved single-aliquot regenerative-dose protocol. *Radiation Measurements*, 32, 57-73.

Murray, A.S. and Wintle, A.G. (2003) The single aliquot regenerative dose protocol: potential for improvements in reliability. *Radiation Measurements*, 37, 377-381.

Murray, A.S., Olley, J.M. and Caitcheon, G.G. (1995) Measurement of equivalent doses in quartz from contemporary water-lain sediments using optically stimulated luminescence. *Quaternary Science Reviews*, 14, 365-371.

Olley, J.M., Murray, A.S. and Roberts, R.G. (1996) The effects of disequilibria in the Uranium and Thorium decay chains on burial dose rates in fluvial sediments. *Quaternary Science Reviews*, 15, 751-760.

Olley, J.M., Caitcheon, G.G. and Murray, A.S. (1998) The distribution of apparent dose as determined by optically stimulated luminescence in small aliquots of fluvial quartz: implications for dating young sediments. *Quaternary Science Reviews*, 17, 1033-1040.

Olley, J.M., Caitcheon, G.G. and Roberts R.G. (1999) The origin of dose distributions in fluvial sediments, and the prospect of dating single grains from fluvial deposits using -optically stimulated luminescence. *Radiation Measurements,* 30**,** 207-217.

Olley, J.M., Pietsch, T. and Roberts, R.G. (2004) Optical dating of Holocene sediments from a variety of geomorphic settings using single grains of quartz. *Geomorphology*, 60, 337-358.

Pawley, S.M., Toms, P.S., Armitage, S.J., Rose, J. (2010) Quartz luminescence dating of Anglian Stage fluvial sediments: Comparison of SAR age estimates to the terrace chronology of the Middle Thames valley, UK. *Quaternary Geochronology*, 5, 569-582.

Prescott, J.R. and Hutton, J.T. (1994) Cosmic ray contributions to dose rates for luminescence and ESR dating: large depths and long-term time variations. *Radiation Measurements*, 23, 497-500.

Singhvi, A.K., Bluszcz, A.., Bateman, M.D., Someshwar Rao, M. (2001). Luminescence dating of loess-palaeosol sequences and coversands: methodological aspects and palaeoclimatic implications. *Earth Science Reviews*, 54, 193-211.

Smith, B.W., Rhodes, E.J., Stokes, S., Spooner, N.A. (1990) The optical dating of sediments using quartz. *Radiation Protection Dosimetry*, 34, 75-78.

Spooner, N.A. (1993) The validity of optical dating based on feldspar. Unpublished D.Phil. thesis, Oxford University.

Templer, R.H. (1985) The removal of anomalous fading in zircons. *Nuclear Tracks and Radiation Measurements*, 10, 531-537.

Thomsen, K.J., Murray, A.S., Jain, M. and Botter-Jensen, L. (2008) Laboratory fading rates of various luminescence signals from feldspar-rich sediment extracts. *Radiation Measurements*, 43, 1474-1486.

Wallinga, J. (2002) Optically stimulated luminescence dating of fluvial deposits: a review. *Boreas* 31, 303-322.

Wintle, A.G. (1973) Anomalous fading of thermoluminescence in mineral samples. *Nature*, 245, 143-144.

Zimmerman, D. W. (1971) Thermoluminescent dating using fine grains from pottery. *Archaeometry*, 13, 29-52.

Wessex Archaeology Ltd registered office Portway House, Old Sarum Park, Salisbury, Wiltshire SP4 6EB
Tel: 01722 326867 Fax: 01722 337562 info@wessexarch.co.uk www.wessexarch.co.uk

FS 606559